1-1-2005

Predictive modeling of surface finish in fine grinding

Yi Yang
Ryerson University

PREDICTIVE MODELING OF SURFACE FINISH IN FINE GRINDING

by

Yi Yang

B.Eng., Huazhong University of Science and Technology, Wuhan, China, 1999

A thesis

presented to Ryerson University

in partially fulfillment of the

requirements for the degree of

Master of Applied Science

in

Mechanical Engineering

Toronto, Ontario, Canada, 2005

I hereby declare that I am the sole author of this thesis.

I authorize Ryerson University to lend this thesis to other institutions or individuals for the purpose of scholarly research.

I further authorize Ryerson University to reproduce this thesis by photocopying or by other means, in total or in part, at the request of other institutions or individuals for the purpose of scholarly research.

Ryerson University requires the signatures of all persons using or photocopying this thesis. Please sign below, and give address and date.

Predictive Modeling of Surface Finish in Fine Grinding

A thesis for the degree of

Master of Applied Science, 2005

by

Yi Yang

Department of Mechanical Engineering, Ryerson University

ABSTRACT

Grinding is one of the important machining processes when tight tolerances and fine surface finishes are required. However, due to the large number of process parameters involved, predicting the outcome of a grinding process is not a trivial task. This thesis describes the development of a predictive model of surface finish in the fine surface grinding process.

The surface topography of a grinding wheel was analyzed using a laser scanner. The statistical distribution for grain protrusion heights and the transverse and longitudinal spacing of grains were determined. Each protruded grain is counted as a cutting edge that engages with the workpiece to generate a unique chip. A solid modeller was used to model an individual chip as an ellipsoid. The measured topography of the grinding wheel, together with a kinematic relationship in surface grinding, was used to determine the geometrical characteristics of the ellipsoid. The solid modeller was then used to model the chip removal process by successive grains.

The surface roughness predicted by the model was compared with experimental results. The results showed good consistency between the model and the actual surface properties.

ACKNOWLEDGEMENT

I sincerely wish to thank my advisors, Dr. Ahmad Ghasempoor and Dr. Jeff Xi, to whom I owe a debt of gratitude for the invaluable guidance and assistance that they so unselfishly rendered throughout this research effort.

I gratefully acknowledge the generous support of the Department of Mechanical Engineering of Ryerson University. I thank them for the use of their facilities during much of the research that has culminated in the successful completion of this project.

The support from my family is greatly appreciated.

Although words can never adequately express the extent of my appreciation for your immeasurable support and encouragement: words are all I have. Thank you.

TABLE OF CONTENTS

Contents **Page**

LIST OF FIGURES

Figure **Descriptions** **Page**

LIST OF TABLES

Table **Descriptions** **Page**

List of APPENDICES

Appendix **Descriptions** **Page**

CHAPTER 1

INTRODUCTION

Grinding is one of the important operations employed in Production Engineering to remove unwanted material and to introduce a desired geometry and surface properties. Most machined components have either been machined by grinding at some stage of their production or have been processed by machines which owe their precision to abrasive operations [1]. Grinding is traditionally regarded as a final machining process in the production of components requiring smooth surfaces and fine tolerances [1].

The development of wear-resistant abrasives, powerful machinery and adequate machining technologies has led to considerably increased efficiency of the grinding process. The economical advantages thus achieved consolidate and extend the position of grinding technology, the grinding process being a quality-defining finish method.

The entire field of grinding may be divided into two regimes [2]:

- Stock removal grinding (SRG)
- Form and finish grinding (FFG)

The first regime, i.e., course grinding, involves those processes in which the main objective is to remove unwanted material without regard for the quality of the resulting surface. The abrasive cut-off operation and the conditioning of slabs and billets in the steel industry are typical processes of this type. In these cases, undeformed chip thickness is relatively large and wheel wear is so rapid that it is not necessary to periodically dress the wheel to remove wear flats and metal adhering to the tool face.

The second regime, i.e., fine grinding, involves those operations in which form and finish are a major concern, and wheels must be periodically dressed to provide sharp cutting edges that are relatively free of adhering metal and wear flats.

Diverse types of grinding operations are also classified according to the shape of the wheel, the kinematic motions of the workpiece, the active grinding wheel surface, the feed direction and the control methods applied. Surface grinding, cylindrical grinding and shape grinding classify the process based on the purpose of the grinding process. Depending on the position of the contact area on the workpiece itself, external grinding and internal grinding are distinguished. The kind of surface to be generated, the kinematics of the machining operation, as well as the shape or the profile of the grinding wheel, are other major characteristic properties of the process [3].

Grinding is performed by refractory abrasive particles of relatively uncontrolled geometry, producing many small chips of random shape. Each abrasive grain is a potential microscopic cutting edge. Due to the multiplicity of cutting edges and their irregular geometry, it is difficult to analyze and gain insight into the mechanism of the grinding process.

Another complicating factor is the large number of parameters that affect the outcome of the process. Based on the quality demands, the machining parameters are determined with the aid of grinding tests, which are both time-consuming and costly.

Process models can contribute significantly to the understanding of the grinding process. Models, if accurate, are economical and efficient ways to predict the result of the process under varying process parameters and, therefore, can reduce the overall manufacturing costs. This thesis deals with one of the important quality characteristics in fine grinding, or namely, surface finish of the part. The quality of the surfaces produced by grinding is judged by surface integrity and surface texture. Surface integrity describes the mechanical and metallurgical damage caused by grinding on the material of the workpiece underneath the work surface. The plastic deformation and the thermal influences on the microstructure which occur during grinding can be revealed by changed degrees of hardness on and underneath the work surface, as well as by metallographic examinations [3]. Surface texture refers to the micro-geometry or three-dimensional topography of machined surfaces, which is usually characterized

by surface roughness, including average roughness, R_a , and peak-to-valley roughness or so called total roughness, R_t. The surface texture in grinding is affected by a large number of process parameters which again interact with each other and complicate any attempts at modeling the outcome.

1.1 Research Objective

The objective of this thesis is to develop a predictive model of surface finish in the fine grinding process. The model will take into consideration the grinding wheel properties and the kinematic relationship between wheel and workpiece.

1.2 Thesis Outline

The thesis is organized in the following chapters:

Chapter 1 is a brief introduction of the research objectives and thesis outline.

Chapter 2 reviews the background and presents an overview of the related research literature.

Chapter 3 describes the experimental set up for capturing the geometry and topography of a grinding wheel using a two-dimensional laser scanner; the method

used to determine the topography of the grinding wheel; the kinematic relationship between the grinding wheel and the workpiece is investigated; the chip model is developed.

Chapter 4 introduces the principle of application for the solid modeler and the generation of the ellipsoid model for chip formation. The simulation program of the grinding process is developed.

Chapter 5 validates the model by comparing the simulated results with measurements.

Chapter 6 contains the conclusions and recommendations for further work.

CHAPTER 2

BACKGROUND AND LITERATURE REVIEW

2.1 Grinding Wheel

A grinding wheel is a bonded abrasive tool composed of hard abrasive grains or grits which play the role of cutting edges. The type of abrasive grain, size of the grit, bond material, and porosity significantly determine the properties and performance of bonded abrasive tools.

Grinding wheels are made from a variety of grit material in a wide range of sizes used with various bond materials and compositions. The wheels are classified as either conventional or superabrasive depending on the material of the abrasive. Commonly used conventional wheels contain either silicon carbide or aluminum oxide abrasive with vitrified or resinoid bonds. Superabrasive wheels contain either diamond or cubic boron nitride (CBN) with vitrified, resin, or metal bonds. The grinding wheels with a variety of wheel shapes and sizes fit the diverse requirements of grinding tasks.

To specify grinding wheels in a standard marking system, the wheel specification

defines the following parameters [3]:

(1) The type of abrasive in the wheel.

(2) The abrasive grain size.

(3) The wheel's hardness.

(4) The wheel's structure.

(5) The bond type.

(6) Any other maker's identification codes.

2.1.1 Abrasive Types

As mentioned earlier, abrasive materials for conventional wheels used are aluminum oxide or silicon carbide.

Many types of abrasives based on synthetic aluminum oxide and two common types of silicon carbide generate different chemical compositions and structural characteristics which affect their physical and mechanical properties. They are widely employed in practice to approach different purposes of grinding.

The abrasive materials for superabrasive wheels include diamond and cubic boron nitride (CBN). As the abrasive material for a superabrasive wheel is expensive, only a relatively shallow section of the active area of the wheel surface actually consists of bonded abrasive, which is attached to a metal or plastic hub [3].

2.1.2 Grain Size

The abrasive grain size is the most important parameter affecting the surface finish. The abrasive grain size is designated by a grit number, which is related to the mesh number of the screen (specified as wires per linear inch) used to sort the grains. The mesh number ranges from 8 – 600 [4]. A larger grit number indicates a smaller grain size. Sieving is generally used for sizing of conventional abrasive grains coarser than 240 grit number. The sieving method consists of passing abrasive grains through a stack of standard sieves from the coarser aperture sieves to progressively finer meshes with increasing mesh number down the stack. Nominally, the aperture size decreases by a factor of $\sqrt{2}$ between adjacent sieves in a stack of standard sieves [3].

A standard grit number is defined in terms of grain sizes corresponding to five such sieves. For example, grit number 46 involves grains caught on sieves number 30, 40, 45, 50 and 60 using a standard sample size and sieve-shaking procedure. The specification requires 0% retention on the #30 sieves (i.e., no grain larger than 595 μm), not less than 70% passing the sieve #40 (not more than 30% in the size range 595~420 μm), not less than 40% retention on #45 (size range 420~354 μm), not less than 65% retention on #40 and #50 combined (size range 420~297 μm), and not more than 3% passing #60 (at least 97% in the size range 595~250 μm) [3].

2.1.3 Wheel Hardness

Wheel harness represents the cutting ability of the wheel compared to the workpiece material. It is scaled in a standard marking system by wheel grade using the letters A to Z. The wheel hardness increases gradually from A to Z. The wheel grade provides general information of wheel strength and the strength with which abrasive grains are held by the bond materials. In general, harder wheels are used for grinding softer material and softer wheels used for harder material. Figure 2-1 shows the hardness for typical abrasive materials.

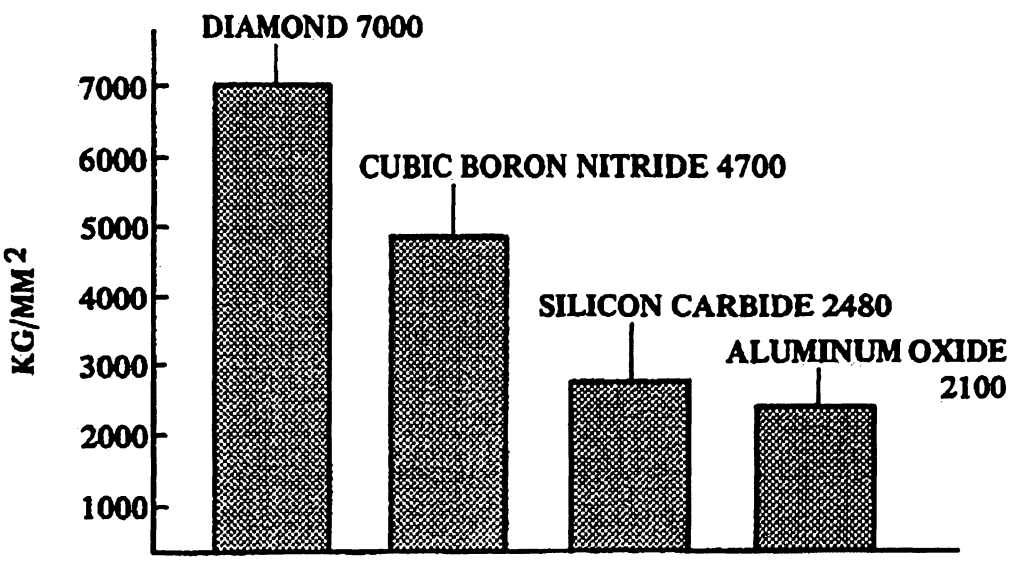

Figure 2-1. Bar chart for hardness of typical abrasive materials [5]

2.1.4 Structure Number

The structure number in the wheel standard marking system indicates the volumetric concentration of abrasive grains in the grinding wheel. The bigger the number, the fewer the abrasive grains or more open the wheel. Structure number is closely related with the grain density, or the grain spacing of the wheel, which affects the wheel topography and the workpiece surface finish. Figure 2-2 illustrates dense, medium and open structures.

An upper limit on the grain concentration (lower limit on structure number) is imposed by packing limitations that refer back to the grain size and its distribution. Abrasives of a given size and shape are characterized by a limiting natural packing density, which can be reached by shaking and application of moderate pressure, low enough so as not to cause grain crushing [3].

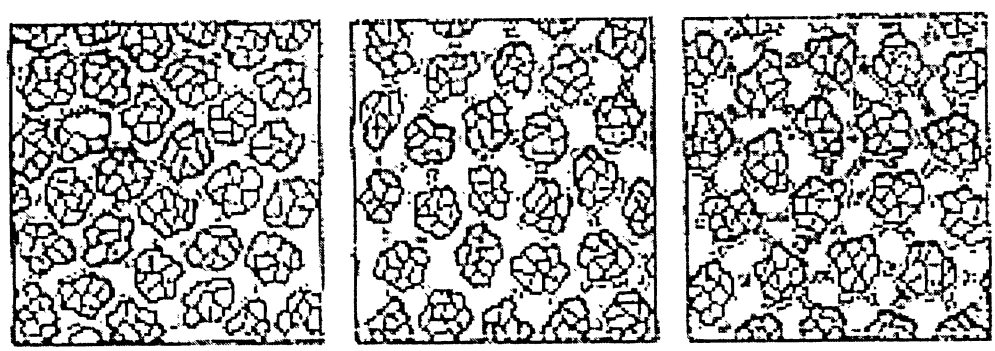

Figure 2-2. Illustration of structures of the grinding wheel[5]

2.1.5 Bond Type

Abrasive grains are embedded in bond material. The bond material is required to be strong enough to withstand grinding forces, temperature, and centrifugal forces without disintegration, while resisting chemical corruption caused by the cooling fluid. The bond material also affects the wheel rigidity, the ability to retain abrasive grains during the cutting operation, as well as the wheel hardness.

Eight types of bond materials for the conventional abrasive wheels are included in the standard marking system. They are: resinoid; resinoid reinforced; shellac; oxychloride; rubber; rubber reinforced; silicate; vitrified. Most conventional abrasive wheels use either vitrified or resinoid bonds. Three types of bond materials for superabrasive wheels are: resin; vitrified and metal.

2.2 Grinding Wheel Topography

The grinding wheel topography is very important in the predictive modeling of the grinding process. The cutting edges which are randomly distributed on the grinding wheel influence not only the grinding forces but also the surface roughness of the workpiece.

2.2.1 Active Cutting Edge

The microstructure of the grinding wheel is composed of numerous individual abrasive grains which are stochastically distributed in the six degrees of freedom. All of them are potential cutting points; however, only partial grains are actually engaged in the cutting operation and are called active cutting edges or grains. Thus, the population of active cutting edges is responsible for the generation of the ground surface.

The number of cutting edges per unit length and their orientation are characteristic quantities of a grinding wheel. One grain may have one or more than one cutting edge; however, it is sufficient to consider the cutting edges that belong to the same grain as one cutting edge [6].

The density of cutting edges and the stiffness of contact are closely related to each other. With the same grade, the density of cutting edges increases with grain size; with the same grain rate, the density of cutting edges increases with grade [7].

The active cutting edges engage with the workpiece, cutting grooves from the workpiece surface. If all the active cutting edges were of the same protrusion heights, the cutting path generated would consists of successive identical scallops [8]. On the other hand, when cutting edges have different protrusion heights, the longer

protrusion grains would generate deeper grooves on the workpiece surface than shorter ones. The cutting path generated would then depend on the engagement of the outmost protruded grains. A predictive model of the grinding process must take into account the random protrusion heights of a typical grinding wheel.

Since the cutting edges on the wheel are randomly distributed and many cutting edges contribute generating the machined surface, a statistical analysis of the distribution and quantity of cutting edges is conducted to describe the necessary configuration of the wheel surface in a deterministic way. Several methods can be used in order to measure the number, size and distribution of cutting edges on a grinding wheel. These include the scanning electron microscope (SEM) stylus instrument and the taper print method, as well as indirect measuring methods such as dynamometer and scratch trace measuring methods.

2.2.2 Grit Shapes

Apart from the number and distribution, the shape of the individual cutting edges is also a characteristic aspect of the grinding wheel used to describe the micro geometry of wheels. It is not sufficient to generate the grinding wheel topography only by counting the number of grains and the measured profiles of the cutting edges.

Since the actual shapes of the cutting edges are highly irregular, a variety of

shape assumptions are made in modeling of the grinding process. Spheres and cones are widely used. In Namba and Tsuwa [9] , the grain shape of the cone is applied to model the belt grinding process, and only the mean value of the conical angles is considered for simplicity. Figure 2-3 shows the sectional structure of coated abrasives. Furthermore, Cooper et al. [10] modeled the grain shape as a frustum of a cone instead of one cone with fixed 90 degrees of conical angle, because a frustum of a cone represents the wear flat on the tip of cone grains by sliding opposite to the workpiece. The wear flats were related to the sharpness of grains. Tooe et al. [11] and Shaw [12] adopted the sphere (semi-sphere) as the shape of grains. Due to its symmetry, this is convenient for the analysis of grinding forces. It also represents a reasonable model because of the large negative rake angles presented by the grains. The normal force applied to a grain was assumed to be similar to the force in the Brinell Hardness test or the Meyer hardness test [13].

For superabrasive wheels, the crystal morphology of diamond and CBN-grits can be described with simple geometrical shapes such as tetrahedrons, cuboids and octahedrons. Warnecke et al. [14] modeled the grit as an octahedron by comparison of SEM images of a single grit, as illustrated in Figure 2-4.

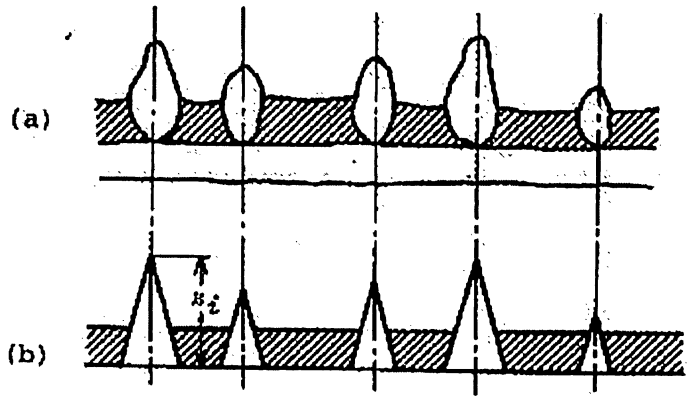

Figure 2-3. Sectional structure of coated abrasive [9]

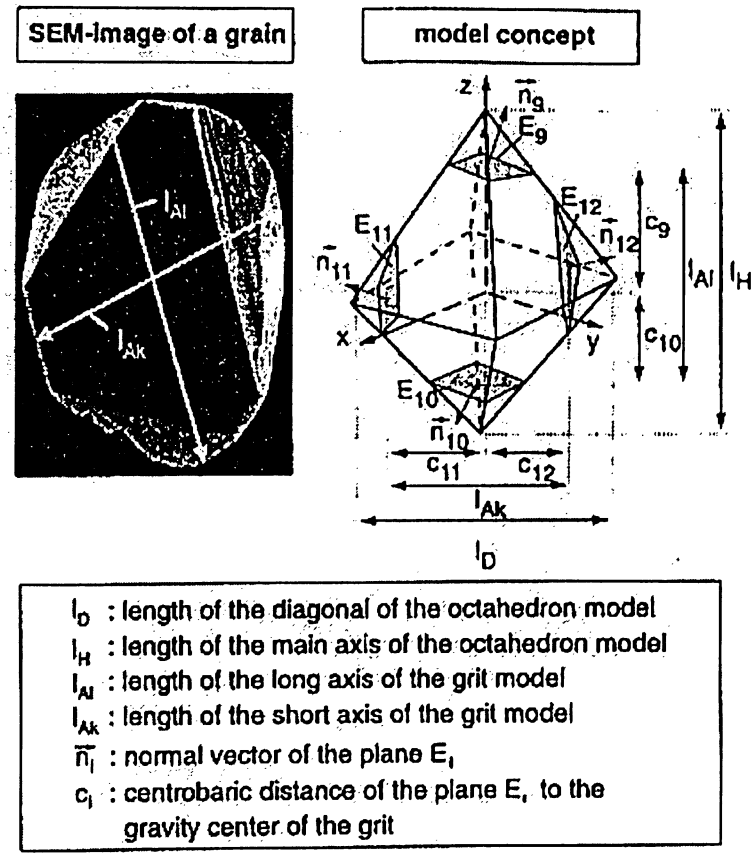

Figure 2-4. Grit shape model of octahedron [14]

2.2.3 Models of Wheel Topography

Due to the important role of the wheel topography in the study of the grinding mechanism, numerous methods have been developed for measuring and characterizing the grinding wheel topography.

The optical profilometer was applied to obtain a three-dimensional representation of the grinding wheel topography by Inasaki [15]. An algorithm was devised to analyze the measured data and identify the grain cutting edges. The cutting edge distribution was presented by a radial depth with reference to the wheel surface. It was concluded that varying truing and dressing conditions, such as fine truing lead, slow-dressing feed, and small truing, as well as small dressing depth, lead to a high cutting edge density.

The basic model derived by Tönshoff [3] for topography based on the kinematic grain count is:

$$N_{kin} = c_{gw}(\frac{1}{q})^{e_1} a_e^{\frac{e_1}{2}} (\frac{1}{d_{eq}})^{\frac{e_1}{2}} \qquad (2\text{-}1)$$

where, N_{kin} is kinematic grain count in units of $1/mm^2$; c_{gw} is a constant for the grinding wheel; q is a speed ratio; a_e is the working engagement in units of mm; d_{eq} is the equivalent diameter of the grinding wheel in units of mm; and e_1 is an exponent. In this model, the shape of the cutting edge is taken into consideration by using a constant. The kinematic grain count has a factor c_{gw} which is independent of the

boundary conditions. Furthermore, the speed ratio, the working engagement and the equivalent diameter have been considered. The various topography models have the common feature that many measurements are required to determine the model parameters. Furthermore, the statistical geometric distribution of the grains is not taken into consideration [3].

The Monte Carlo method was employed by Yoshikawa et al. [16] to estimate the fundamental wheel parameters such as grain spacing on the grinding wheel, undeformed chip geometry and generated surface profile. Also statistical analysis was utilized to calculate the distribution of these parameters from the wheel geometry. The distribution of grains on the wheel was represented by the co-ordinates (X, Y, Z), which were the position of axial, peripheral and radial directions of the wheel, respectively. It was assumed that X has a uniform distribution; Z has a distribution whose density is proportional to the depth of the grits protruded from the wheel surface; Y has a uniform distribution. This assumption leads to an exponential distribution for ΔY, which is the interval of successive appearance of grains for a fixed point in the workpiece. For the i-th grain, the grain co-ordinate can be expressed as [16]:

$$\begin{aligned} X_i &= \alpha R_{3i-2} \\ Y_i &= Y_{i-1} + \beta \log(R_{3i-1}) \\ Z_i &= \gamma \sqrt{R_{3i}} \end{aligned} \tag{2-2}$$

where R is a random number uniformly distributed between 0 and 1, α, β and γ are the constants related to grinding conditions.

A wheel which is meshed with the interval of the grain is described in [8]. The grains are equally oriented in the x, y and z directions by a constant grain interval Δ which can be determined by:

$$\Delta = 137.9M^{-1.4}\sqrt[3]{\frac{\pi}{32-S}} \quad (mm) \tag{2-3}$$

where M is the grit number and S is the structure number. Figure 2-5 illustrates the meshing of the grinding wheel. The grain protrusion heights follow by a normal distribution density function with the mean value and standard deviation expressed by:

$$\mu = 68M^{-1.4}$$
$$\sigma = (15.2M^{-1} - 68M^{-1.4})/3 \tag{2-4}$$

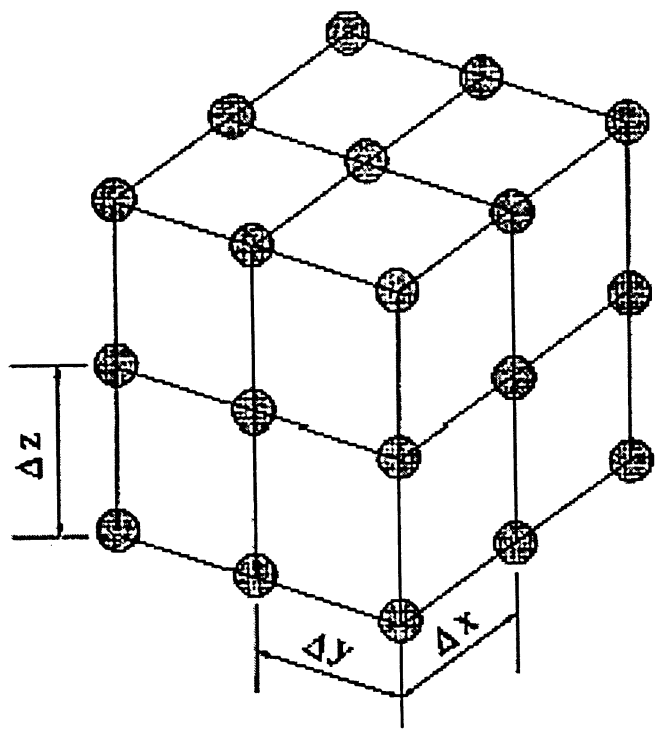

Figure 2-5. Illustration of meshed grinding wheel in [8].

The wheel surface topography is established in Badger et al. [17] by taking into account either the number of active cutting asperities per unit area of the grinding wheel or the distribution of the slopes of the asperities. These two parameters, the asperity peak density and asperity slope, were used to quantify the sharpness of the wheel.

2.3 Chip Formation

Chip formation and material removal depend to a large degree on the microstructure of the grinding wheel, the relative motion and the geometric parameters of the process.

The material fed into the contact area, with a given working engagement due to the workpiece peripheral speed, is equal to the material flowing out that is related to the cutting speed and the equivalent chip thickness. One of the characteristic parameters is the sum of all individual chip thicknesses in the contact area between grinding wheel and workpiece. For a single grain, the maximum chip thickness equals the maximum thickness of the theoretical chip. The single-grain approach is based on the assumption that during chip formation, no plastic deformation and no plowing occurs at the edge of the trace. Thus, for chip formation, the equivalent chip thickness is used to determine the process parameters of the machine tool to meet the quality demands relevant to a specific machining application [3].

2.4 Applications of Solid Modeler

Solid modelers have been used in the simulation of machining processes [18][19][20]. Spence et al. [18] developed a comprehensive physical machining process simulation program for use in process planning applications, as well as factory floor monitoring and control. The system is based on extensions to the ACIS solid modeling kernel. Models for both flat end and ball nose tools are implemented, and multi-axis motion is supported. A special sweep representation is used to generate the solid necessary for Boolean subtraction and part model updating. Figure 2-6 shows the process of workpiece updating. As the solid body in (a) moves along the cutting path, a Boolean subtraction removes the swept volume from the part model, as shown in (b) and (c); then the data geometry of the part model is updated and (d) shows the final updated part after machining by the Boolean operation.

Wang et al. [20] presented the method to model swept volume by computing a family of critical curves from a moving solid. The swept volume is considered as the totality of all points that belong to the trace of a moving solid, which is called a generator.

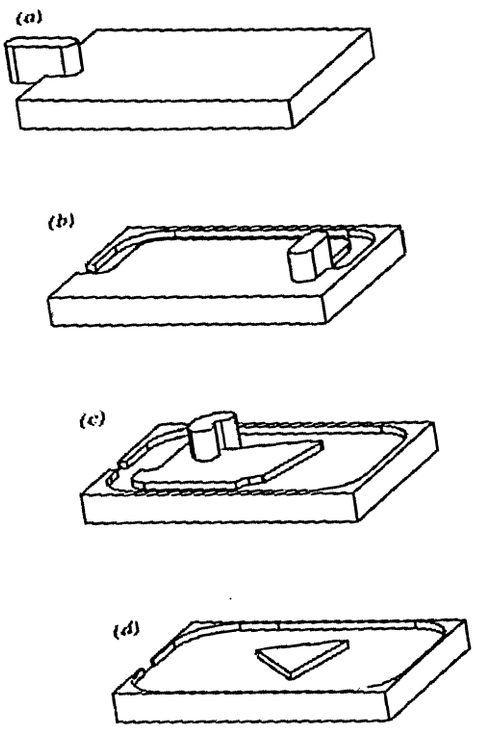

Figure 2-6. Illustration of workpiece updating [18]

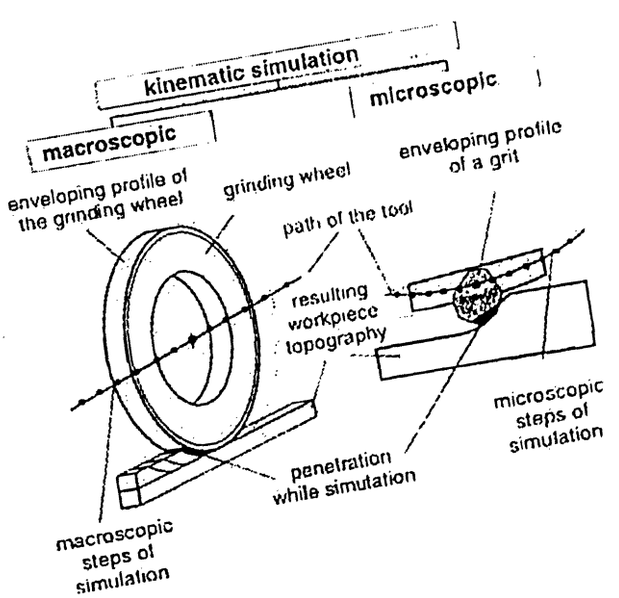

Figure 2-7. Principle of the kinematic simulation [14]

2.5 Kinematic Relationship

The kinematic simulation is based on the numerical three dimensional geometry models of the grinding wheel and the workpiece as shown in Figure 2-7. These models describe the macro- and micro-geometry of the grinding wheel and the workpiece, depending on the degree of abstraction. Together with mathematical models describing the relative motion between the grinding wheel and the workpiece, as well as the kinematic engagement conditions of a single grit, grinding processes can be reproduced as the cumulation of multiple grit engagements. Furthermore, the ideal kinematics can be superimposed with the thermo-mechanical and dynamic effects in the contact area for different grinding technologies [14].

The work presented in the thesis is an attempt to overcome some of the shortcomings of the previous models by simulating a three dimensional solid modeler, in contrast to previously used two dimensional methods. The chips are modeled as solid ellipsoids, generated according to the kinematic relationship between the grinding wheel and the workpiece. The geometric parameters are determined by the characteristic of the grinding wheel and the kinematic relationship. After the chips are removed and the workpiece finish surface updated, the workpiece topography is retrieved by a ray tracer.

CHAPTER 3

METHODOLOGY

Overview

The proposed methodology is presented in this chapter. First, a solid model of a single chip is developed. The topography of the grinding wheel, together with kinematic relationship between the wheel, individual chips and workpiece, is then used to model the chip removal by successive grains. The resulting surface provides a predictive model of the surface finish after grinding.

Due to the complexity of the grinding process, the following assumptions are made for simplification:

- The vibration of the grinding wheel is negligible.
- The elastic-plastic deformation of cutting grains is negligible, the material of the workpiece engaged with cutting edge is totally removed out of the workpiece.
- No slide flow, built-up-edge phenomena [3].
- Grinding wheel wear is not considered.

3.1 Chip Formation

The chip removal process in grinding can be divided into three phases: rubbing, plowing and cutting. When grain engages with the workpiece in up-cut grinding, the grain slides without cutting on the workpiece surface due to elastic deformation; this is the rubbing phase. As the stress between the grain and workpiece increases beyond the elastic limit, plastic deformation occurs which is known as the plowing phase. As plowing continues, the workpiece material piles up on front and sides of the grain to form a groove. A chip is formed when the workpiece material can no longer withstand the shear stress; the chip formation stage is also known as the cutting phase [13]. Figure 3-1 shows the three stages of chip generation.

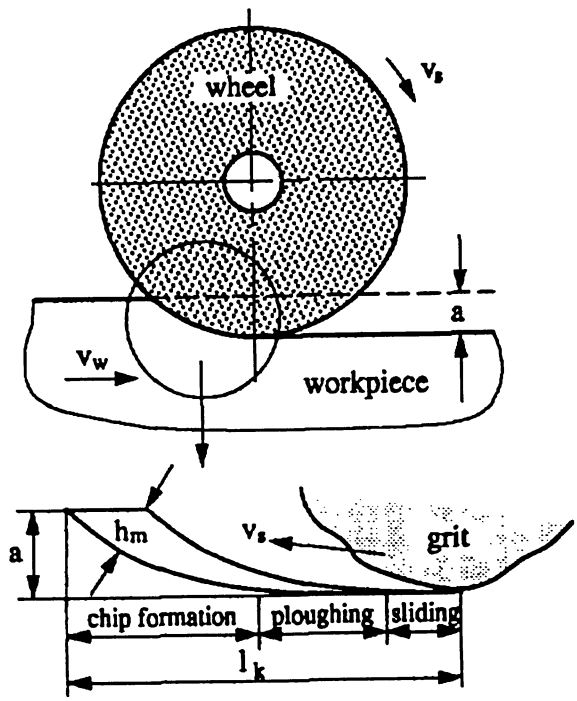

Figure 3-1. Three stages of chip generation [13]

3.1.1 Geometry of a Chip

Chips generated by the engagement of cutting grains into the workpiece surface create a groove that remains on the finished surface as a fingerprint [21]. Therefore, the cross section of the chip created by a single cutting grain is identical to that of the cutting grain itself. Most researchers have used the cone and the sphere as models of a cutting grain. In [22], a trapezoid is used to model the cross section of the undeformed chip.

In the current work, the cross section of the chip is assumed to be an ellipse, as illustrated in Figure 3-2. This is believed to better represent the cross section of a typical grinding chip by combining the cone shape and the sphere shape. The grain is simulated as a curve, such as sphere. The height of the cutting grain, c, is equal to the major semi-axis of the ellipse. Since, in general, the cutting grain is not symmetrical, the cross section of the cutting grain is composed of two half ellipses. The lengths of semi-axes are b_l for left ellipse and b_r for the right one.

3.1.2 Cutting Trajectory of a Single Grain

Figure 3-3 shows the surface grinding process. A wheel of diameter r, rotating with a peripheral velocity of V_s and a translational relative velocity of V_w relative to workpiece, cuts the material. The moving direction of the grinding wheel center is

parallel but opposite to the moving direction of the workpiece.

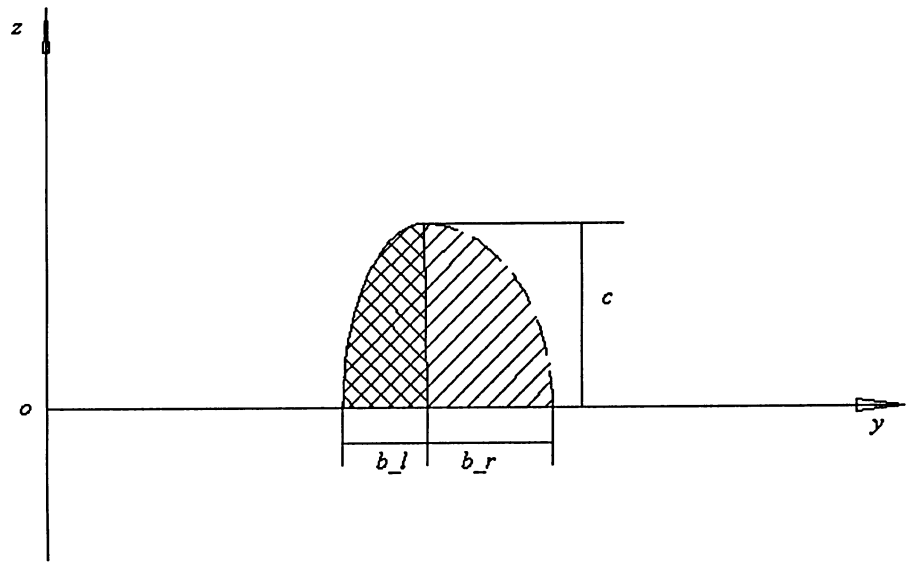

Figure 3-2. Cross section of cutting grain

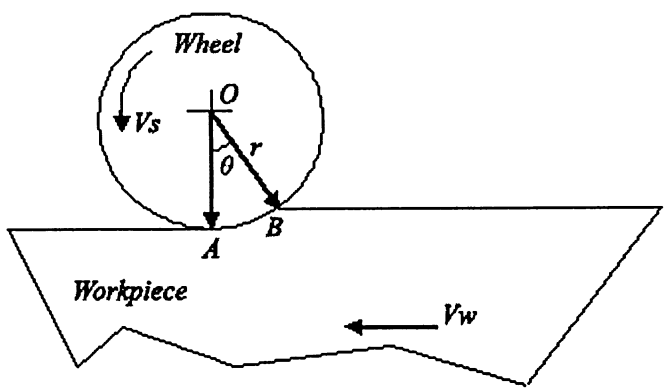

Figure 3-3. Illustration of straight surface grinding

In order to research the grinding mechanism, the kinematic relationship of a single grain engaged with the workpiece is analyzed. As shown in Figure 3-4, A is the cutting point of a single grain on the wheel surface. The position of grain A can be described as:

$$\begin{cases} x = v_w t + r\sin\theta \\ y = r(1-\cos\theta) \end{cases} \tag{3-1}$$

where x and y are the coordinates of grain A in a Cartesian coordinate system, r is the radius of the grinding wheel, t is time, and θ is the rotation angle of the wheel in the interval of time t. Since θ is very small, the following approximations can be made:

$$\sin\theta \approx \theta \tag{3-2}$$

and

$$\theta^2 \approx 2(1-\cos\theta) \tag{3-3}$$

At the same time,

$$v_s = r\omega \tag{3-4}$$

and

$$\theta = \omega t \tag{3-5}$$

where ω is the angular velocity of the grinding wheel. Therefore,

$$v_s t = r\theta \tag{3-6}$$

Substituting equation (3-6) into equation (3-1) and using the approximation equation (3-3), the equation (3-1) can be re-arranged as,

$$\begin{cases} x = r\theta(\dfrac{v_w}{v_s} + 1) \\ y = \dfrac{1}{2}r\theta^2 \end{cases} \tag{3-7}$$

The trajectory of a single cutting grain can be derived by eliminating the variable θ in equation (3-7), i.e.,

$$\frac{y}{x^2} = \frac{1}{2r(\frac{v_w}{v_s}+1)^2} \tag{3-8}$$

Re-arranging equation (3-8) yields,

$$y = \frac{rx^2}{2(r+\frac{v_w}{v_s})^2} \tag{3-9}$$

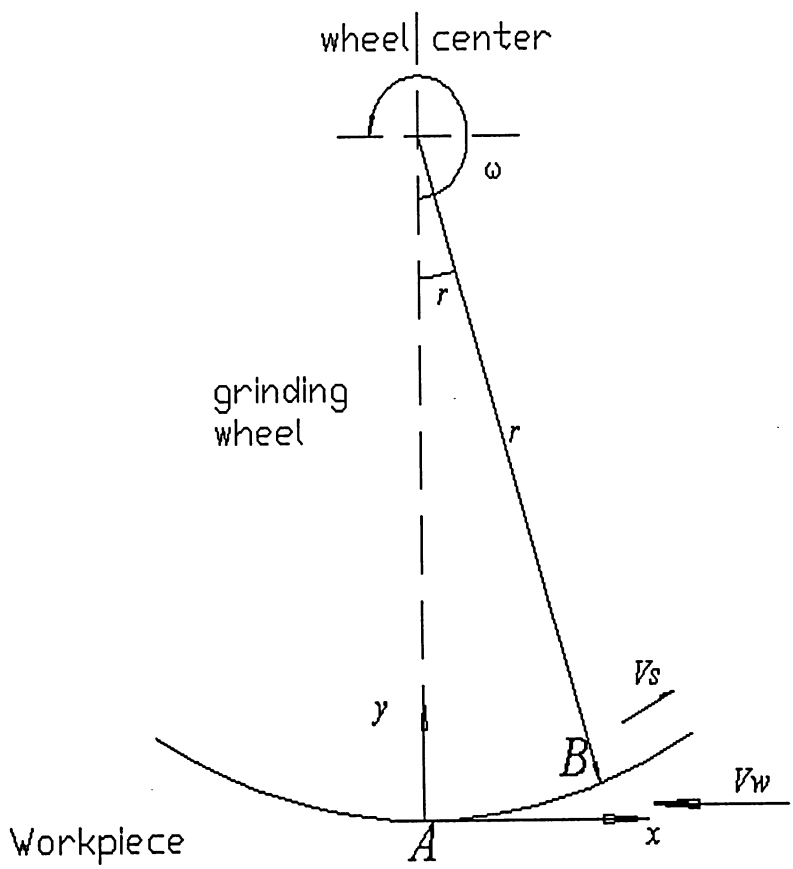

Figure 3-4. Illustration of the kinematic geometry of single grain

For the case of grains with the identical heights, all the grains engaged with the workpiece make the identical depth of dents on the workpiece as shown in Figure 3-5.

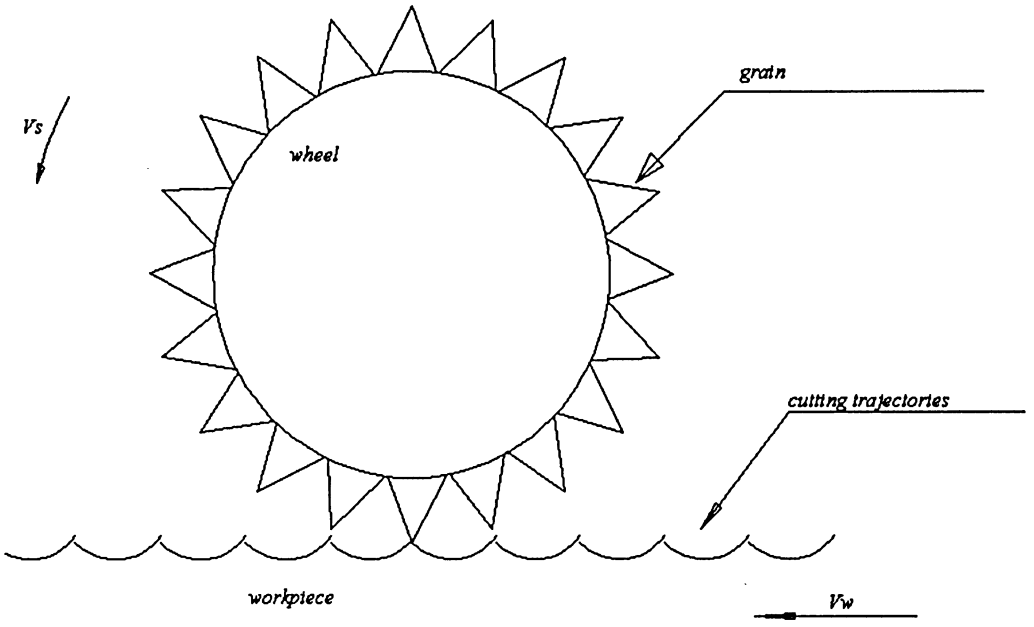

Figure 3-5. The cutting trajectories by identical height of cutting grains

However, the protrusion heights of cutting edges are randomly distributed. To reflect this, equation (3-9) can be expressed for each cutting grain with a different protrusion height as:

$$y_i = \frac{r_i x^2}{2(r_i + \frac{v_w}{v_s})^2}, \tag{3-10}$$

Here,

$$r_i = r_s + \Delta r_i \tag{3-11}$$

where r_s is the nominal radius of the grinding wheel, Δr_i is the protrusion height of

the cutting grain to the neutral level of wheel for the i^{th} protruded grain.

Equation (3-10) can be rewritten as:

$$y = \alpha x^2, \tag{3-12}$$

with α equal to,

$$\alpha = \frac{r_i}{2(r_i + \frac{v_w}{v_s})^2} \quad . \tag{3-13}$$

Equation (3-12) defines a parabola. Re-arranging equation (3-12) yields:

$$x = \sqrt{\frac{y}{\alpha}} \tag{3-14}$$

Furthermore, the co-ordinates of the points A and B in Figure 3-4 for an arbitrary cutting grain can be presented as: $A(x_A, y_A)$, *and* $B(x_B, y_B)$. The co-ordinate of point A is obviously $A(0, 0)$. For point B:

$$y_B = \Delta r_i \tag{3-15}$$

and x_B can be calculated from (3-14) as:

$$x_B = \sqrt{\frac{\Delta r_i}{\alpha}} \quad , \tag{3-16}$$

Thus, the co-ordinate of point B can be express as: $B(\sqrt{\frac{\Delta r_i}{\alpha}}, \Delta r_i)$.

While Equation (3-10) represents a satisfactory two-dimensional model of trajectory of a single chip, it cannot be used directly for a three-dimensional model of the chip form in grinding. It is proposed that the segment of the parabola AB be modeled as a

quarter of an ellipse. This would allow a three-dimensional model of the chip to be an ellipsoid. The approximation of the parabola in Equation (3-10) with a section of an ellipse is reasonable because the engagement range of a single cutting grain intersecting with the workpiece is very short in the x-axis. This engagement range depends on the cutting depth Δr_i, the nominal radius r_s, the velocity of workpiece V_w and the peripheral velocity V_s of the grinding wheel. The segment of the parabola AB in Figure 3-3 is approximated as a quarter of an ellipse in which the length of the semi-long axis (See Figure 3-6) is equal to

$$a = \sqrt{\frac{\Delta r_i}{\alpha}}, \tag{3-17}$$

and the length of semi-short axis is expressed as:

$$c = \Delta r_i \tag{3-18}$$

Using Equations (3-17) and (3-18), the equation for the ellipse can be written as:

$$\frac{x^2}{a^2} + \frac{(y-c)^2}{c^2} = 1, \tag{3-19}$$

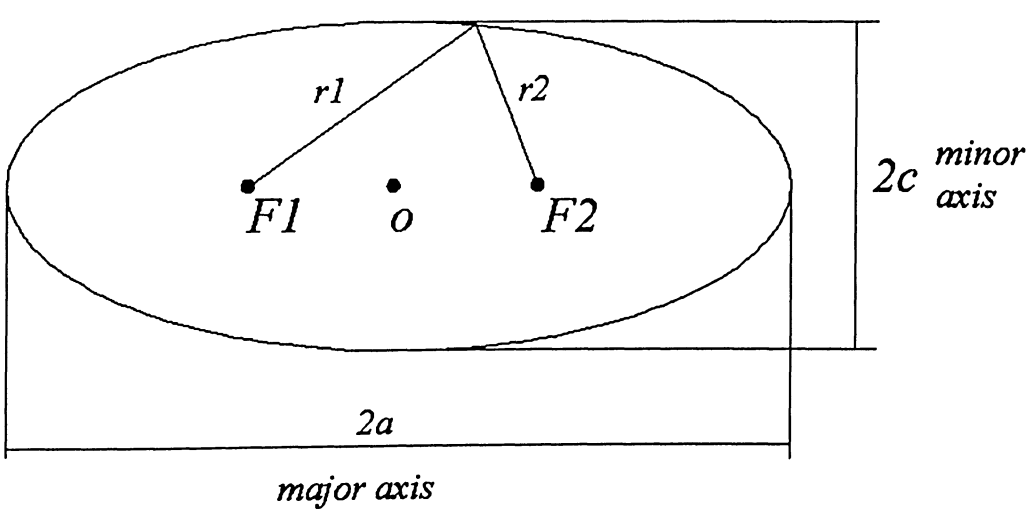

Figure 3-6. Illustration of geometry of an ellipse

The quarter ellipse is defined by the coordinates:

$$\begin{cases} x \geq 0 \\ y \leq c \end{cases}. \tag{3-20}$$

To verify the hypothesis of replacing the parabola with the ellipse, the plots of an ellipse and a parabola are compared in Figure 3-7. The parameters are set as follows: $r_s = 0.09m$, $\Delta r_i = 1 \times 10^{-5} m$, $v_w = 0.06m \cdot s^{-1}$, $v_s = 42.5m \cdot s^{-1}$. Substituting these parameters into equations of (3-13), (3-14), (3-16), (3-17), (3-18), the parabola function yields:

$$y = 10.80x^2; \quad x \in (0, 10^{-3})m \tag{3-21}$$

The ellipse can be expressed as:

$$\frac{x^2}{(10^{-3})^2} + \frac{(y - 10^{-5})^2}{(10^{-5})^2} = 1; \quad x \in (0, 10^{-3})m, \quad y \in (0, 10^{-5})m \tag{3-22}$$

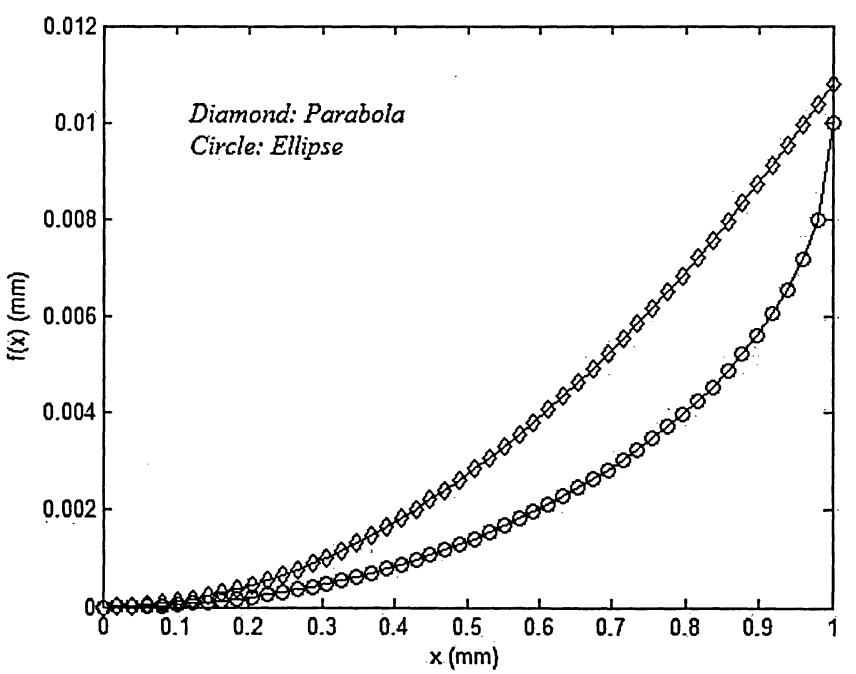

Figure 3-7. The comparison of the plots of ellipse and parabola

As shown in Figure 3-7, the diamonds represent the parabola as expressed in equation (3-21), and the circles show the ellipse for equation (3-22). From the plots, it is evident that the hypothesis of the cutting trajectory for a single grain is correct, i.e., states that the cutting trajectory of a single grain can be regarded as an ellipse instead of a parabola, when x lies in a very small interval, e.g., $\{0-10^{-3}m\}$. The difference between the two curves is within $10^{-6}m$.

3.2 Generation of Chip Model

As discussed above, the cross section of the chip formed by a single grain is modeled as part of an ellipse. An observation of Figure 3-7 indicates that it might also be possible to represent the trajectory of the cutting point by an ellipse. This would make it possible to use an ellipsoid to represent a solid model of the chip, because for any ellipsoid, as illustrated in Figure 3-8, arbitrary intersection parallel to the y-z plane is an ellipse, which corresponds to the shape of a single grain intersection. Also, arbitrary intersection parallel to the x-y plane is also an ellipse, which corresponds to the elliptic trajectory made by a cutting grain.

Therefore, the three-dimensional chip generated by a single grain can be modeled as an ellipsoid.

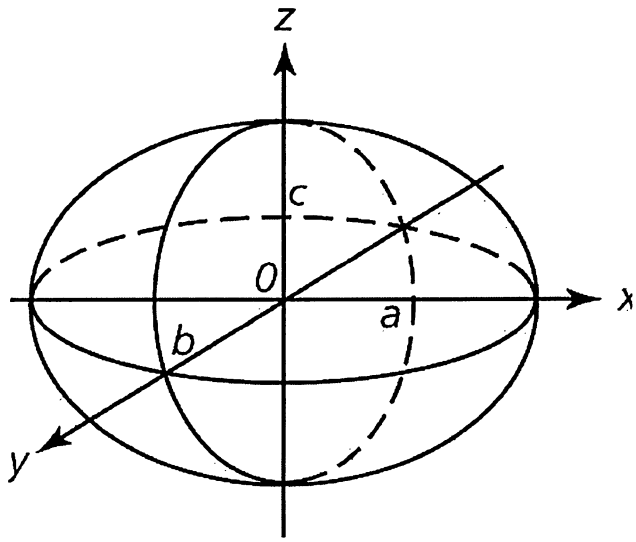

Figure 3-8. Geometry illustration of an ellipsoid

The general formula for an ellipsoid is:

$$\frac{(x-x_0)^2}{a^2}+\frac{(y-y_0)^2}{b^2}+\frac{(z-z_0)^2}{c^2}-1\le 0 \tag{3-23}$$

where x, y and z are the Cartesian coordinates (see Figure 3-8). $p(x_0, y_0, z_0)$ is the coordinate for the centre of the ellipsoid, and a, b, and c are the semi axis lengths in the x, y, and z directions, respectively. The choice for parameters a, b, and c are dictated by wheel topography and cutting conditions, which determine the kinematics of the chip-wheel interaction. Parameter a is related to the length of the chip, parameter b is related to the width of the cutting grain, and parameter c is related to the protrusion height of the cutting grain. The width and protrusion height of the cutting grain can be measured from the wheel, while the chip length is determined by cutting conditions including wheel diameter and cutting speeds. The wheel topography is discussed first and then the kinematics of the cutting process is described.

3.3 Wheel Surface Topography

Researchers have used a variety of models to characterize the wheel surface topography. As discussed previously, direct measuring methods include the taper print method and the stylus methods. Indirect measuring methods include SEM, dynamometer and scratch trace-measuring methods.

In this study, a non-contact laser profilometer was used. The laser profilometer uses the triangulation principle to detect the changes in height (See Figure 3-9). For specifications of the laser profilometer, refer to Appendix A. Computer controlled drivers move the beam in a linear path. In order to scan the surface of the grinding wheel, a measurement setup, shown in Figure 3-10, was used.

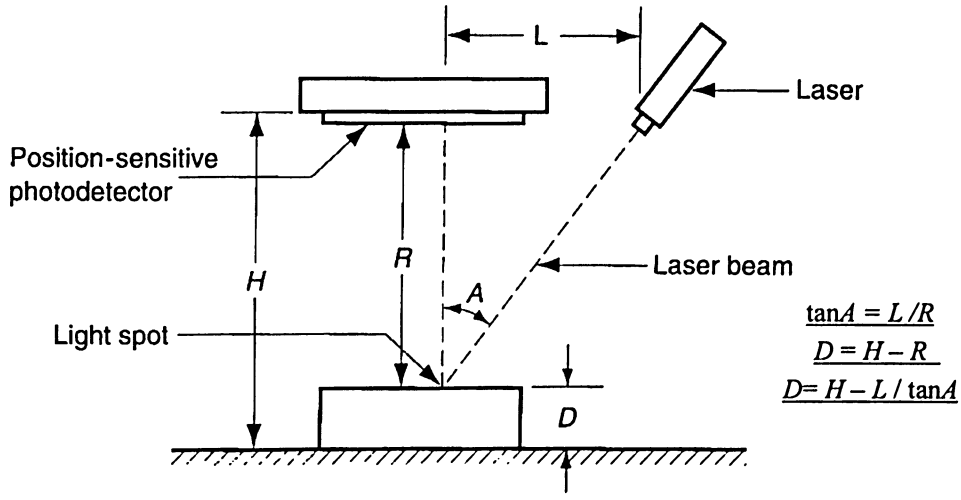

Figure 3-9. Principle of laser profilometry

The grinding wheel is held in a three-jaw chuck attached to a divider head. This arrangement allows an angular resolution of 0.184°. An aluminum oxide grinding wheel with grit number of 60 and vitrified bond was used for these measurements. The specification of the measured grinding wheel was 89A60J8AV217. The overall dimensions of the wheel were $25.4mm \times 25.4mm \times 177.8mm$. Figure 3-11 shows an example of the scanned grinding wheel profile.

The information which can be extracted from these profiles includes grain protrusion height and width distribution.

3.3.1 Protrusion Height Distribution

It has been shown that the pattern of the wheel topography is transferred, with some modifications, to the workpiece surface [15]. Therefore, a comprehensive analysis of the wheel topography would benefit the predictive modeling of the workpiece surface finish. When the cutting grains are considered to be of identical height from the bond level, the predicted roughness values are three orders of magnitude smaller than what is obtained experimentally [1]. Thus the presumption of the identical protrusion height cannot predict the finished surface roughness accurately. For a more realistic model, the statistical distribution of protrusion height must be considered.

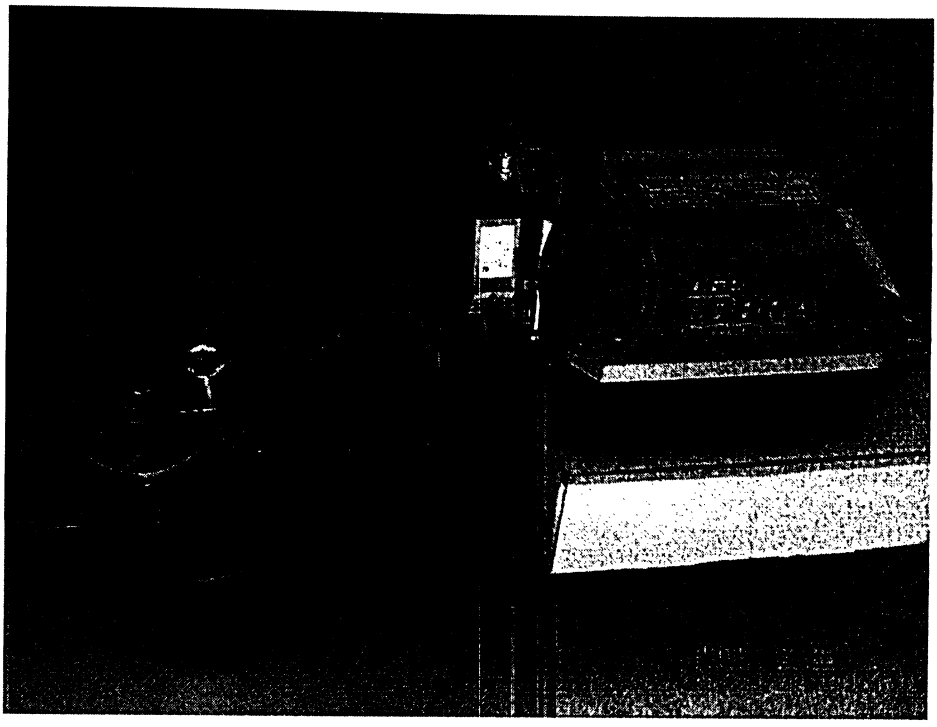

Figure 3-10. Experiment set-up for measuring wheel topography

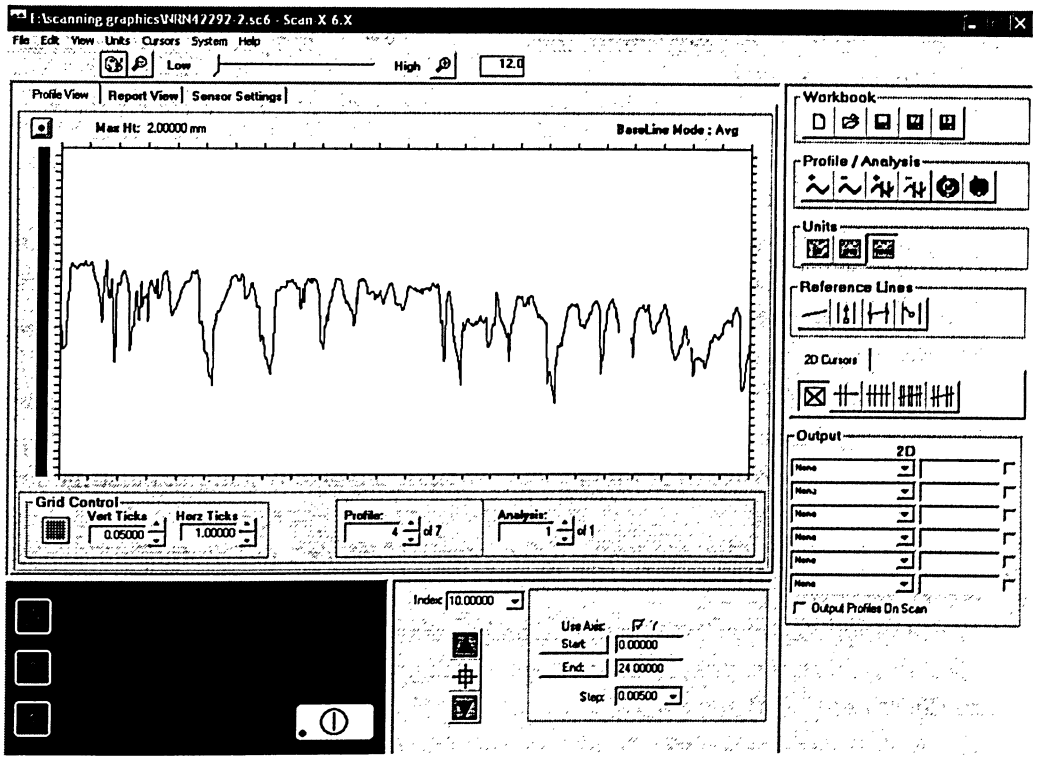

Figure 3-11. A scanned grinding wheel profile in ScanX interface

An approximate measure of protrusion height of cutting grains can be obtained based on the average grit size and its standard deviation. Since each nominal grit size includes a range of abrasive particle sizes, the grit dimension corresponding to a particular grit number might be characterized by an average value. The grit dimension d_g is often quoted according to the relationship [1]:

$$d_g(mm) = 15.2M^{-1}$$
$$or \qquad (3\text{-}24)$$
$$d_g(inches) = 0.6M^{-1}$$

This approximates the grit dimension d_g as 60% of the average spacing between adjacent wires in a sieve whose mesh number equals the grit number M. When based upon the control sieve opening, the grain dimension can be approximated by [1]:

$$d_{g\max}(mm) = 28M^{-1} \qquad (3\text{-}25)$$

the average dimension of the grain can be approximated by [1]:

$$d_{gavg}(mm) = 68M^{-1} \qquad (3\text{-}26)$$

Figure 3-12 shows the abrasive grain dimensions as obtained from above equations. In general, when grit number is less than 46, d_g is smaller than d_{gavg}, As soon as grit number exceeds 46, d_{gavg} starts to be smaller than d_g. The probability distribution used with the grain protrusion height is typically a normal distribution [8]. In order to ensure the accuracy of the proposed model, the protrusion height of a typical grinding wheel was measured and its distribution and averages were compared to Equations (3-24) and (3-26).

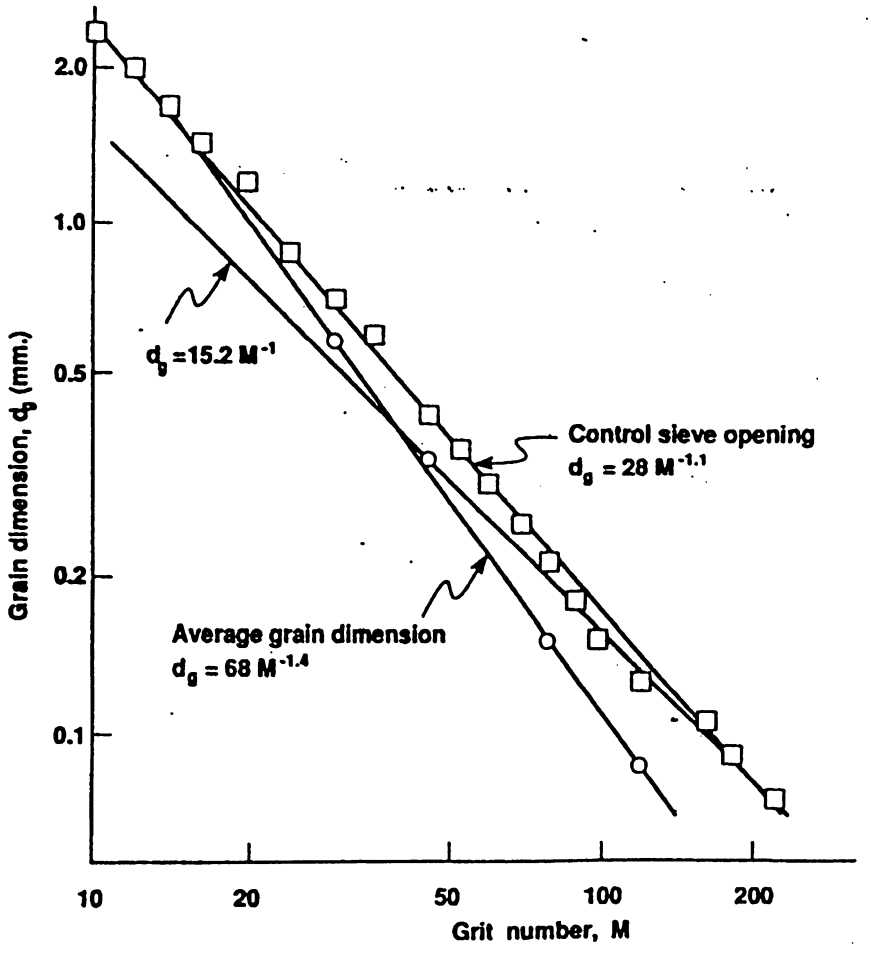

Figure 3-12: Grain dimension versus grit-number based on sieve wire spacing, control sieve opening and grain dimension [1]

The laser profilometer was used to measure the protrusion height distribution of the grinding wheel. The data file generated by the scanning process was analyzed in order to extract the probability density function which best describes the distribution. For each set of data, the baseline was established and the height measurement was relative to this baseline. For the case of multi-cutting edges in a protruded grain, the so-called pseudo cutting edges are filtered and removed using a reference value d_{ref}, which is set to be half of the average grain size d_{gavg}[1]. The average grain size is

related to sieves used, as calculated by equation (3-26). Figure 3-13 shows how this is applied. Grain size d_1 is considered valid since d_1 is greater than $d_{ref.}$ However the grain size d_2 will be disregarded because d_2 is less than $d_{ref.}$ Therefore, the next grain size will be calculated as d_3. The result is that only the biggest protrusion height will be taken into account within the range of the reference value d_{ref}; others will be ignored.

The best-matched probability distribution function and parameters were determined from each measured profile of grinding wheel surface as shown in Figure 3-14. The probability distribution of the protrusion height of the grains was found to be essentially a Gaussian distribution within 10% error. This was also verified by chi-square goodness-of-fit test. The maximum d_{max_m} and mean d_{avg_m} of the protrusion height measured are listed in Table 3-1 and compared to the maximum grain protrusion height d_{max} and the average grain protrusion height d_{avg} calculated by Equations (3-22) and (3-24). The relative error for d_{max_m} to d_{max} is 6.77% and the relative error for d_{avg_m} to d_{avg} is 14.10%. The relative errors are within the difference of two adjacent grain size grades, thus, the measured grain size is accepted for simulation, the mean of the average grain protrusion height is $0.251mm$ with a standard deviation of $0.0118mm$.

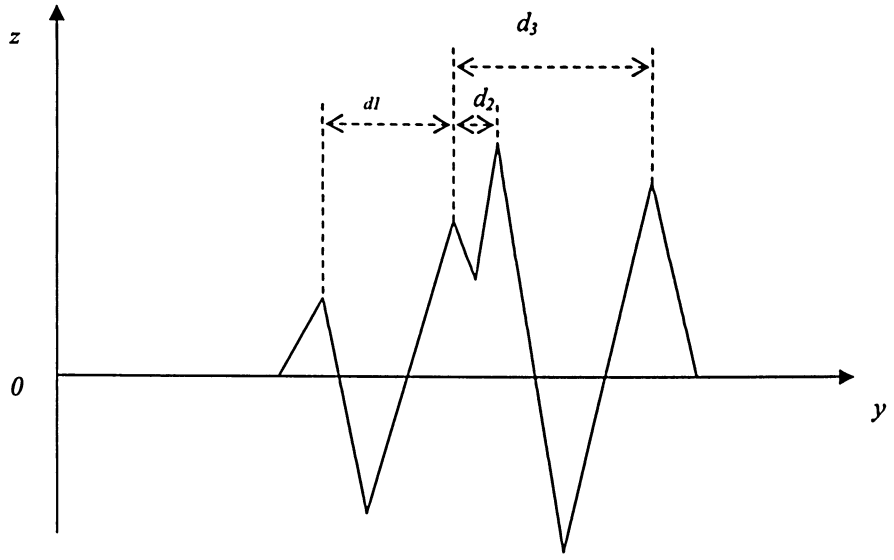

Figure 3-13. Illustration of the calculation of grain size

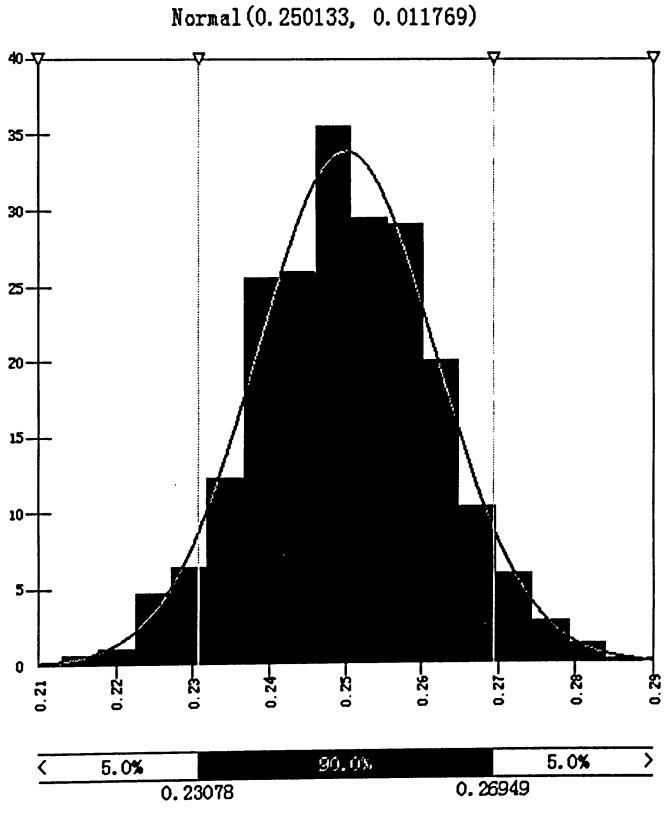

Figure 3-14. Probability distribution fitting of grinding wheel profile

Table 3-1. Measured and calculated grain protrusion heights and grain sizes

Grit Number	Theoretical value		Measured value	
	$d_{max}(\mu m)$	$d_{avg}(\mu m)$	$d_{max\_m}(\mu m)$	$d_{avg\_m}(\mu m)$
60	310	220	289	251

3.3.2 Protruded Grain Spacing Distribution

Another parameter in wheel topography which will affect the chip formation and ultimately the surface finish is the grain spacing. This is related to the density of the wheel. While in some studies constant grain spacing is used, e.g. [8], in the current study, the measured profile was used to experimentally determine the probability distribution of grain spacing. Figure 3-15 shows the definition of the grain spacing, Δy_i.

The distance between adjacent grain tips, Δy_i, was analyzed to find the probability distribution. The results showed that Δy_i also follows a Gaussian distribution with a mean value roughly equal to a quarter of h_{avg}, i.e.,

$$f(\Delta y) = \frac{1}{\sigma\sqrt{2\pi}} \exp\left[-\frac{1}{2}\left(\frac{\Delta y - \mu}{\sigma}\right)^2\right] \tag{3-27}$$

where the mean value $\mu \approx \frac{1}{4} h_{avg}$, and σ is the standard deviation of the interval of adjacent nodes.

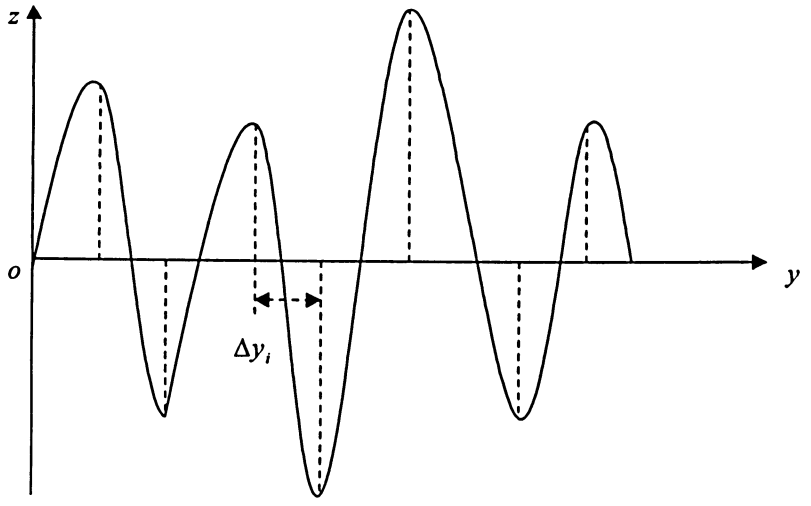

Figure 3-15. Illustration of traverse grain spacing

3.3.3 Grain Sequence

In a typical grinding wheel, the tips and valleys of abrasive grains are located on the surface of the grinding wheel randomly. In the model presented in this thesis, tips and valleys of grains are distributed alternatively relative to the baseline of grinding wheel. Based on this, four types of possible traverse grain profiles are modeled as in Figure 3-16.

These four types of grain profiles are distributed in equal probabilities, conforming to the uniform probability distribution. Thus, they are symbolized by uniformly distributed integers U(1,4) generated by a pseudo-random number generator [23]. For a profile of type 1, the grain profile starts from the baseline

followed by a sequence of tips and then valleys. The integer *1* is assigned to indicate type-1 profile. For a profile of type 2, the grain profile starts with tips and followed by valleys, the integer *2* is assigned to indicate type-2 profile. For a profile of type 3, the grain profile starts from the baseline followed by a sequence of valleys and then tips, the integer *3* is assigned to indicate type-3 profile. For a profile of type 4, the grain profile starts with valleys and followed by tips, the integer *4* is assigned to indicate a type-4 profile.

3.3.4 Regeneration of Wheel Topography

The statistical models of grain height distribution and spacing can be used to regenerate the grinding wheel topography using Monte Carlo simulation. This eliminates the need for measuring each grinding wheel before the predictive model can be used. The measured probability distributions of the protrusion grain height and traverse spacing is used in generating the pseudo-random numbers which regenerate the wheel topography. The circumferential spacing is considered constant along the circumferential direction of the grinding wheel used on the assumption of spatial structure of grain orientation in [8].

Figure 3-17 shows the simulated wheel topography with the mean grain size of 251 μm and standard deviation of 11.8 μm.

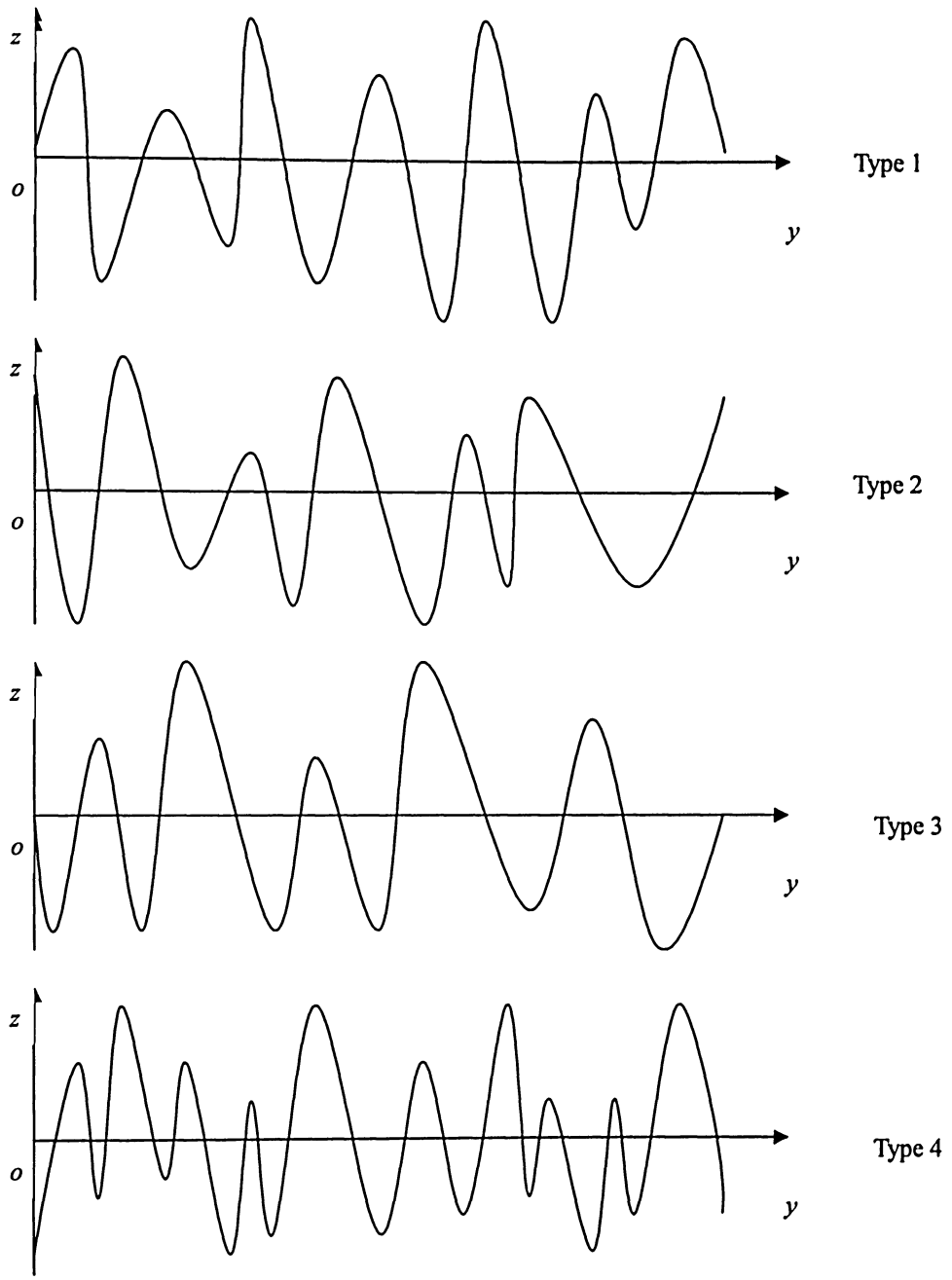

Figure 3-16. Demonstration of grain sequence

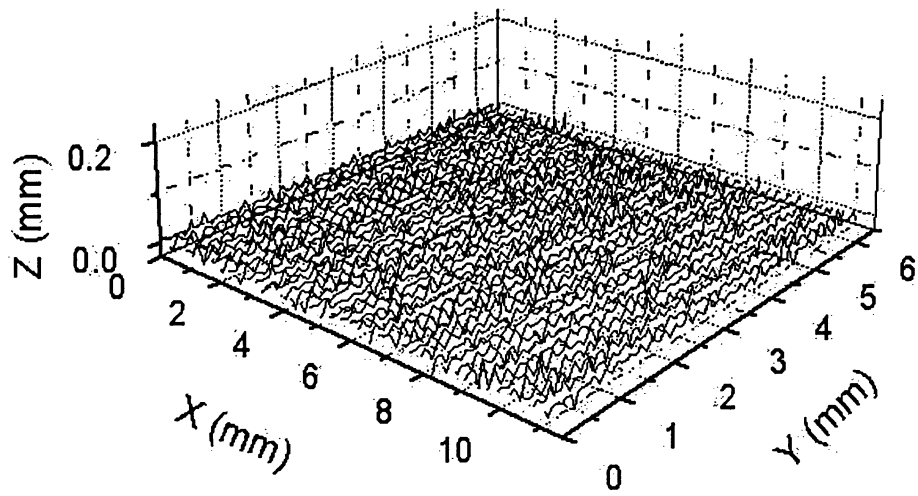

Figure 3-17. The simulated wheel topography

3.4 Transform of Circumferential Interval for Adjacent Grains onto Workpiece

As discussed earlier, rows of traverse grains are oriented along the circumferential direction with a constant interval Δx. As illustrated in Figure 3-18, adjacent grains G1 and G2 are located with distance of Δx in circumferential direction.

At time t_0, the first grain G1 contacts the workpiece in o coordinate, after time interval of Δt, in o' coordinate, G2 starts to engage with the workpiece. The center of the grinding wheel moves from point o to point o', the displacement of the center of the grinding wheel $\Delta x'$ presents the interval for adjacent row of grains engaging onto the workpiece surface.

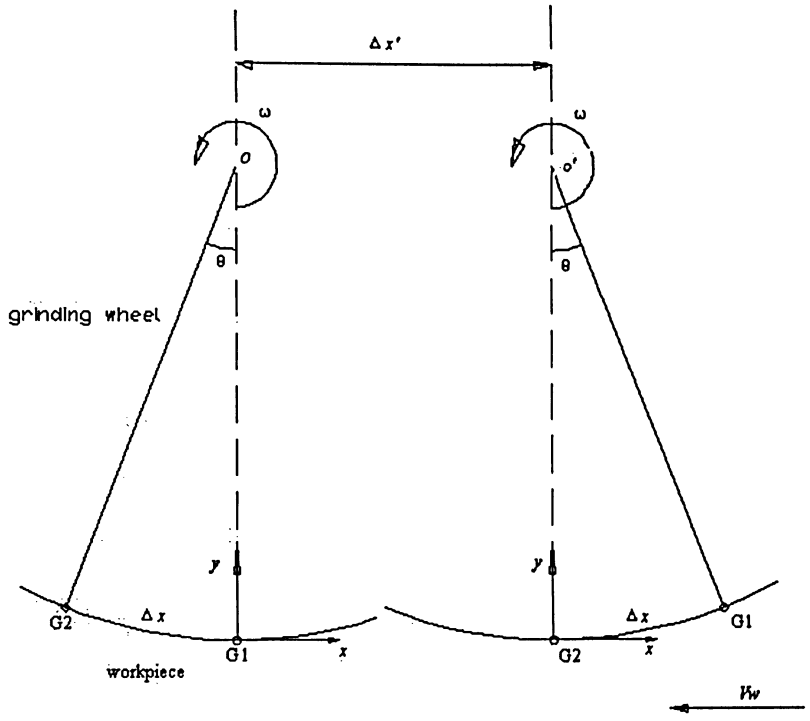

Figure 3-18. Geometry of cutting path for adjacent grains engaged with workpiece

By the kinematic relationship of the adjacent grains, $\Delta x'$ can be derived as follows: within time interval of Δt,

$$\Delta x = v_s \cdot \Delta t \tag{3-28}$$

Δt can be determined as:

$$\Delta t = \frac{\Delta x}{v_s} \tag{3-29}$$

furthermore the displacement of $\Delta x'$ is related with the velocity of the workpiece, because the grinding wheel is fixed to the movement of x direction, thus $\Delta x'$ can be expressed as:

$$\Delta x' = v_w \cdot \Delta t \tag{3-30}$$

equation (3-30) can be rewritten as:

$$\Delta t = \frac{\Delta x'}{v_w} \tag{3-31}$$

combining equations (3-31) and (3-29) yields:

$$\Delta x' = \frac{v_w}{v_s}\Delta x \tag{3-32}$$

Equation (3-32) shows that the adjacent protruded grains with distance of Δx on the circumference of the grinding wheel will start to be engaged onto the workpiece with the horizontal interval of $\Delta x'$, which is proportional to the velocity of workpiece v_w and inversely proportional to the rotating velocity of the grinding wheel v_s.

Thus the distance of the i^{th} protruded grain contacting with the workpiece surface to that of the first one can be expressed as:

$$\Delta x'_i = i\frac{v_w}{v_s}\Delta x, \tag{3-33}$$

where i is an arbitrary integer from 1, 2, 3...

As stated earlier, protrusion height and transverse spacing correspond with parameters c and b in the ellipsoid model of the chip (See Figure 3-8). The parameter c is related to chip length which in turn is dependent on the kinematics of cutting process.

CHAPTER 4

SOLID MODELER AND SIMULATION

Overview

Solid modelers have been used as a vital CAD/CAM tool in recent years. Early applications of solid modeler were limited primarily in generating graphic displays and calculating mass properties [20]. In more recent applications, generating finite element meshes for engineering analysis and numerical control (NC) codes for machining has been introduced [20]. Solid modelers have also been used for simulation of machining processes such as milling and turning. The solid model of the grinding chip developed in previous chapter, in conjunction with a solid modeler, will be used to generate a three-dimensional, predictive model of surface finish in grinding process.

4.1 Principle of Solid Modeling

A solid modeler is essentially a collection of computer algorithms for representing solid objects. These algorithms can be used to generate different models, work out their volumes, add or subtract them to or from other solid models, etc. SvLis which is an efficient set-theoretic geometric modeler was used to develop the

three-dimensional predictive model of the grinding process [24]. SvLis is straightforward enough for any technical person who knows C++ work with, but it is also sufficiently rich in operations and entities to be able to represent a very wide range of shapes for all aspects of engineering. It is user-extendible and provides safe function calls to give access to all its internal geometric structures.

4.1.1 Set-theoretic Modeling

As stated, SvLis is a pure set-theoretic geometric modeler. It treats geometry as a three-dimensional Venn diagram. SvLis can assemble simple solids to create more complicated solids by the set-theory operations. Table 4-1 is the list of four types of operators for set-theoretic modeler.

Table 4-1. List of operators for set-theoretic operations

Operation	Mathematical Operator	SvLis Notation
Union	∪	|
Intersection	∩	&
Difference	− .	−
Symmetric Difference	Δ	^

The usual two-dimensional Venn diagram for all these is shown in Figure 4-1. Intersection returns the part of space where the two objects being intersected are both

solid, just as the logical operator ***AND*** when applied to two binary variable returns 1 only when both variables are 1. Similarly, union returns solid where either or both of the two objects being united are solid, just as the logical operator ***OR*** returns a 1 when either or both of the two binary variables are 1. As seen in Figure 5-1, the relationship between the symmetric difference and intersection is complemental.

Subtraction and Symmetric Difference operators are expressed in SvLis respectively as:

$$A - B = A \cap \overline{B}$$
$$A \wedge B = (A \cap \overline{B}) \cup (B \cap \overline{A}) \tag{4-1}$$

where the bar means set-complement.

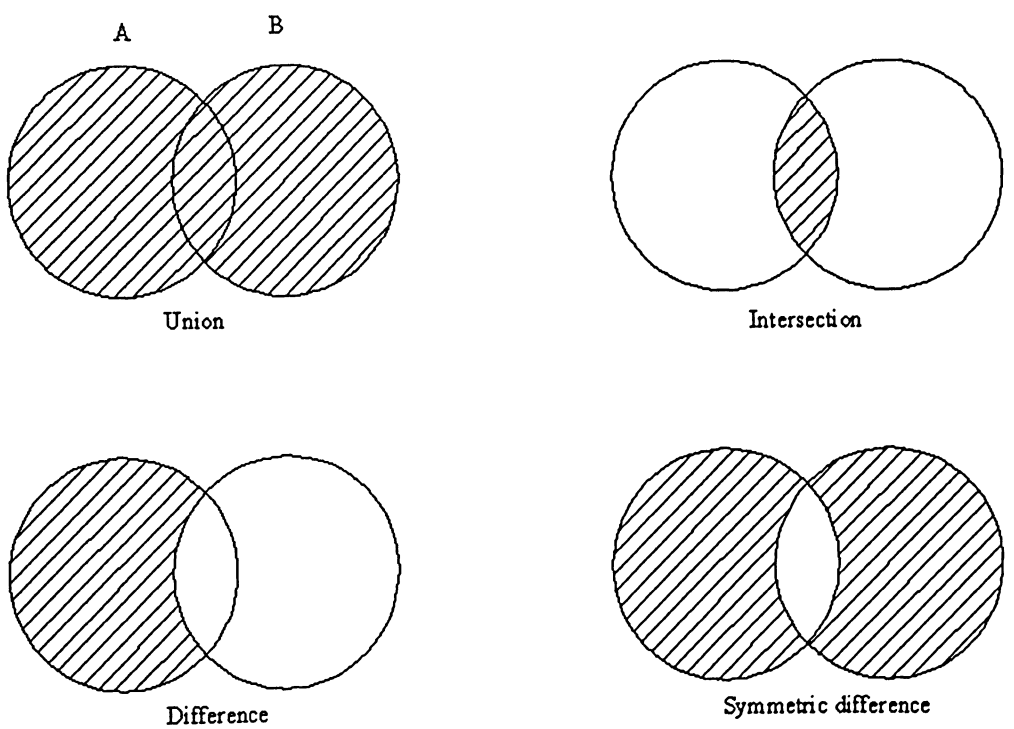

Figure 4-1. Venn diagram for set-theoretical operations [24]

4.1.2 Primitives and Structure Hierarchy

SvLis set-theoretic operations can be expressed algebraically, e.g.,

$$((a \,\&\, b) - (c \mid d) \wedge e \tag{4-2}$$

It can also be represented as a tree structure, as shown in Figure 4-2. The solids *a*, *b*, *c*, *d* and *e* that are located on the root of the tree cannot be broken down into simpler solids and are known as primitives. In other words, a primitive in SvLis is a solid that can not be broken down into simpler solids.

The hierarchy of structures in SvLis is represented graphically in Figure 4-3. Primitives are at the bottom of the hierarchy; sets, which may be just one primitive or a combination of many primitives, are next. A model can contain one or more sets.

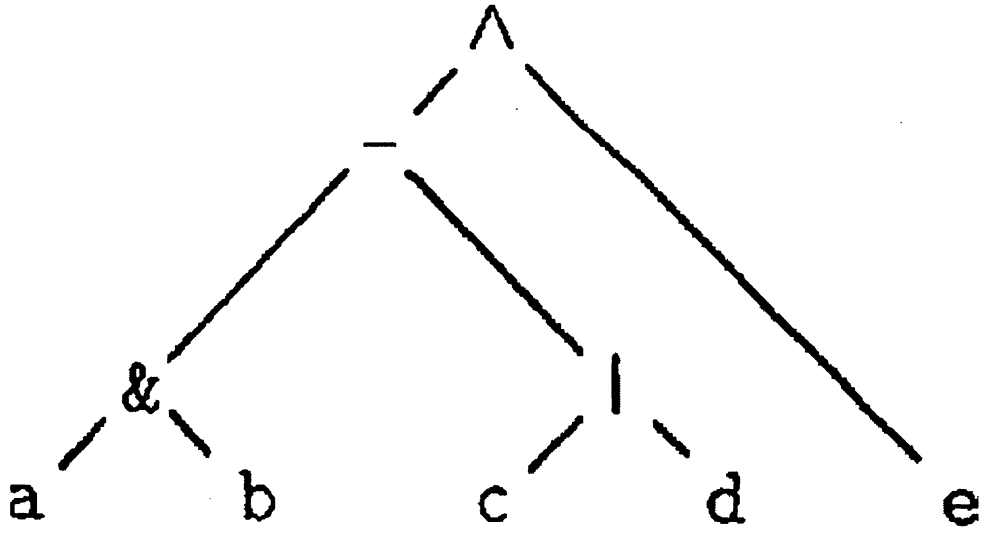

Figure 4-2. An expression tree to illustrate the definition of primitive [24]

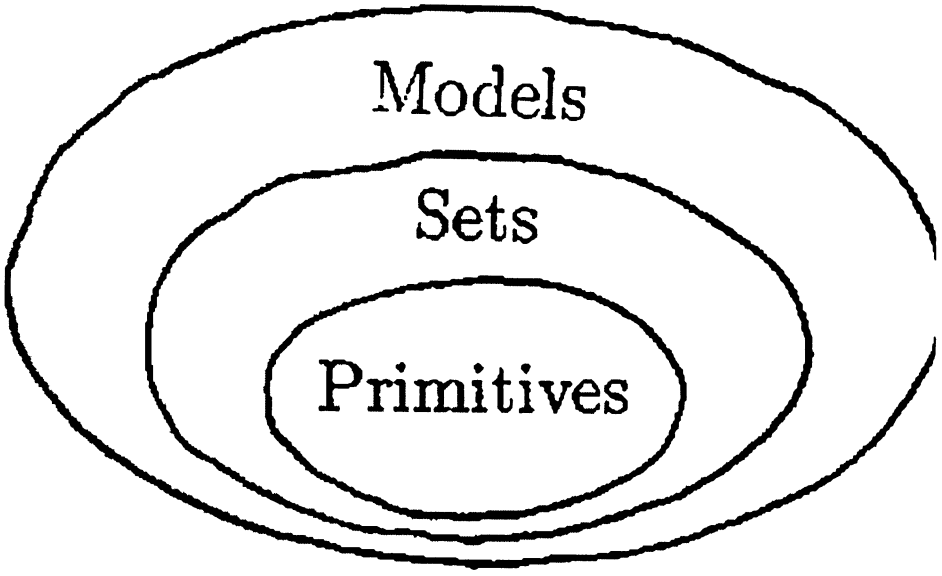

Figure 4-3. The hierarchy of the major SvLis structures [24]

4.2 Creation of Ellipsoid by Solid Modeler

SvLis solid modeler is able to handle a wide range of primitives with curved surfaces. Considering an ellipsoid, with three semi-axis on x, y and z axes as a, b, and c, and with the center located at $p_0(x_0, y_0, z_0)$, the inequality for the solid ellipsoid can be represented in Cartesian coordinate as:

$$\frac{(x-x_0)^2}{a^2}+\frac{(y-y_0)^2}{b^2}+\frac{(z-z_0)^2}{c^2}\le 1. \tag{4-3}$$

This can be rewritten as:

$$f(x,y,z)=\frac{(x-x_0)^2}{a^2}+\frac{(y-y_0)^2}{b^2}+\frac{(z-z_0)^2}{c^2}-1, \tag{4-4}$$

for an arbitrary point in space with the coordinate $p(x, y, z)$, if,

$$f(x,y,z) < 0 \tag{4-5}$$

the point is outside of the ellipsoid; if,

$$f(x,y,z) = 0 \tag{4-6}$$

the point is located on the surface of the ellipsoid, and if,

$$f(x,y,z) < 0 \tag{4-7}$$

the point is within the ellipsoid.

Figure 4-4 shows an ellipsoid created by SvLis solid modeler and representing the inequality,

$$\frac{x^2}{5^2}+\frac{y^2}{4^2}+\frac{z^2}{3^2}-1 \le 0 \tag{4-8}$$

The center is located at point $p_0(0, 0, 0)$, and the lengths for three semi-axes are 5, 4 and 3. In Figure 4-4, ellipsoid (2) is the ellipsoid (1) after it has been cut by *x-y* plane; ellipsoid (3) is ellipsoid (2) cut by *y-z* plane, and ellipsoid (4) is ellipsoid (3) cut by *x-z* plane.

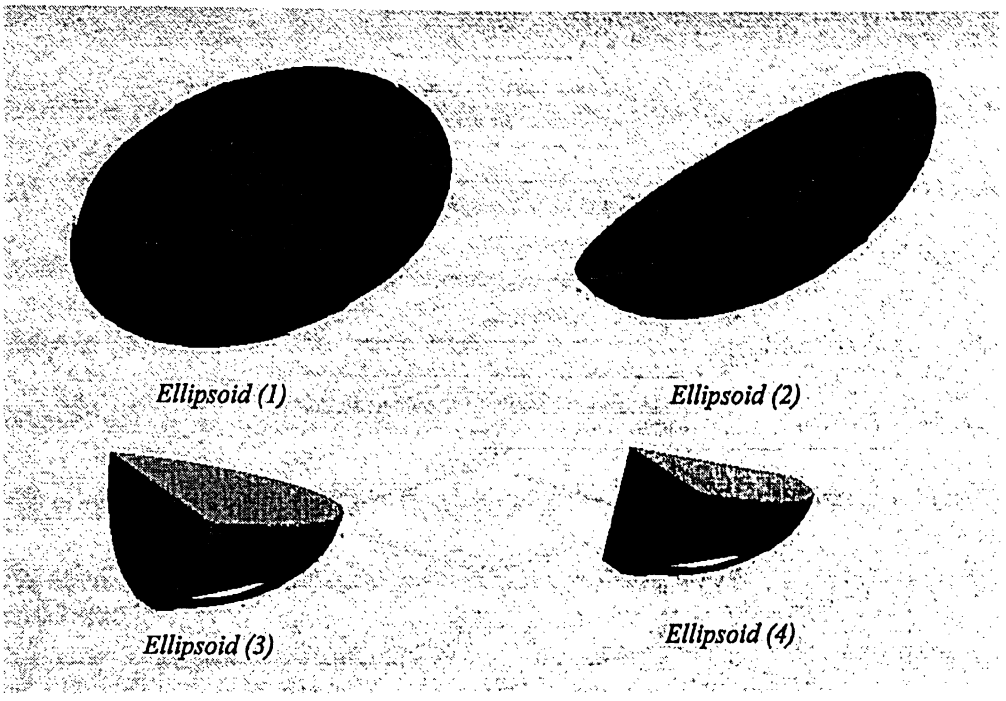

Figure 4-4. Illustration of ellipsoids generated by SvLis solid modeler

4.3 Predictive Model of Surface Finish

The solid model of a single chip developed in Chapter 3 was used to create a predictive model of the surface finish in grinding. Since SvLis is written in C++, the model algorithm was also implemented in C++. The flow chart of the algorithm is shown in Figure 4-5.

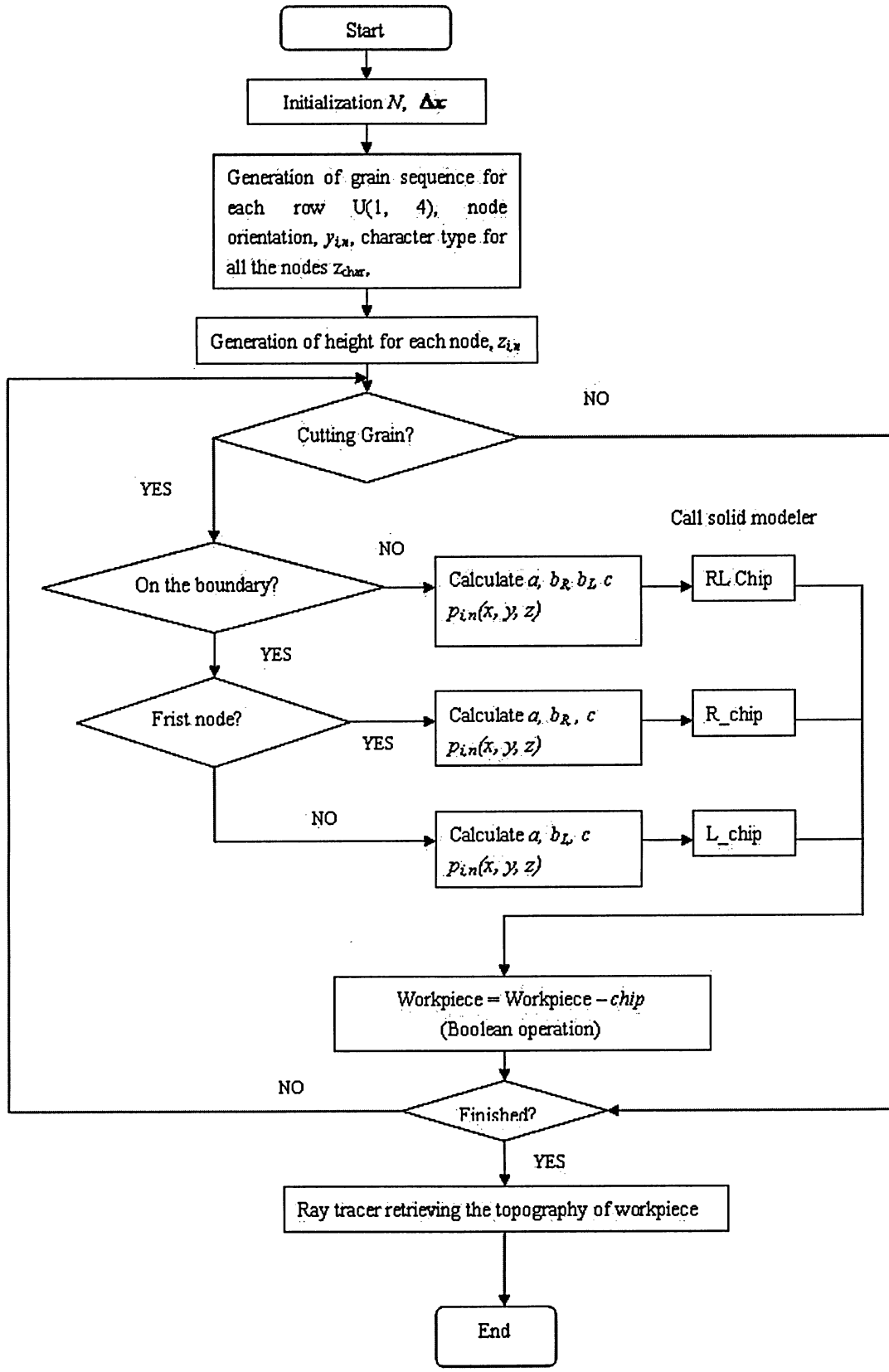

Figure 4-5. Flow chart of grinding process simulation

The algorithm starts by collecting the initial parameters, these are number of rows in circumferential direction: N and the distance between adjacent rows of grains: Δx. The distance Δx between adjacent rows of grains (See figure 2-5) is calculated using

$$\Delta x = \Delta\theta \cdot r_s \tag{4-9}$$

where, $\Delta\theta$ is the angular resolution of three-jaw chuck, and r_s is nominal radius of the grinding wheel. *N*, which represents the number of rows of cutting grains along the circumference of grinding wheel, is also calculated using

$$N = round(\frac{2\pi r_s}{\Delta x}) \tag{4-10}$$

Next is to randomly generate 4 types of grain sequences. As stated in section 3.3.3, uniformly distributed integers U(1,4) are applied to indicate these 4 types of grain profiles with different grain sequences (also see figure 3-17).

As shown in figure 4-6, the points that the grain profiles intersect with baseline and the projection of the tips and valleys from the grain profiles to baseline are called nodes. Nodes are used for grain locating. Starting from the first row of cutting grains, the nodes are allocated along *y*-direction using a normal probability distribution similar to the one obtained during wheel surface topography measurements.

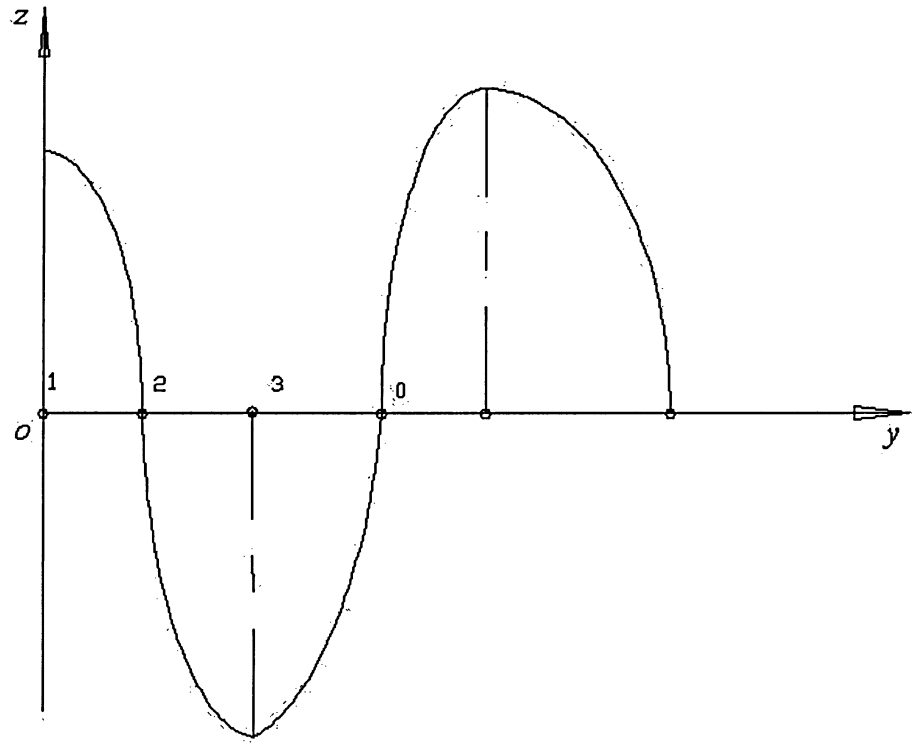

Figure 4-6. Illustration of nodes projected from grain profile on y axis

Once the grain sequence for a grain profile is generated, the property of nodes is determined at the same time. The property of the nodes is indicated by an integer as shown in Figure 4-6. Integer 0 and 2 mean this node is on the baseline of the profile, it is the intersecting point between grain profile and baseline; integer 1 and 3 mean this node is the projection point of the tip or valley from grain profile to baseline. By judging the node property integer, the heights of the nodes are assigned, zeros are assigned to the nodes with integers 0 or 2, and positive generated normally distributed random numbers are given to the nodes with integers 1, as well, negative normally distributed random numbers to the nodes with integers 3.

The next step is to scan the nodes and judge the integer assigned to the node, in the sequence of node by node and row by row. If the characteristic integer of the node judging is integer 1, showing that is a tip point of a cutting grain, and if the tip point is located in the boundary where,

y =0,

as shown in Figure 4-7, the distance between the node *0* to node *1* can be calculated as

$$b_r = y_1 - y_0, \tag{4-11}$$

In this case, the R-type ellipsoid module is called to generate the chip. If the cutting grain is not located on the boundary, the R-L combined ellipsoid module is applied. For example, if the i^{th} grain is a cutting grain, the distance between node i and node i-*1* and the distance between node i+*1* and node i are calculated. These are substituted in to the R-L combined ellipsoid module with parameters of

$$b_l = y_i - y_{i-i} \tag{4-12}$$

and

$$b_r = y_{i+1} - y_i, \tag{4-13}$$

The workpiece solid model is updated with the application of the Boolean subtraction operation, essentially removing the generated ellipsoids. In the third case, the tip node is the last node of that row, node n. In this case, the L-type ellipsoid module is called using:

$$b_l = y_n - y_{n-i} \tag{4-14}$$

The three types of ellipsoids are shown in Figure 4-8.

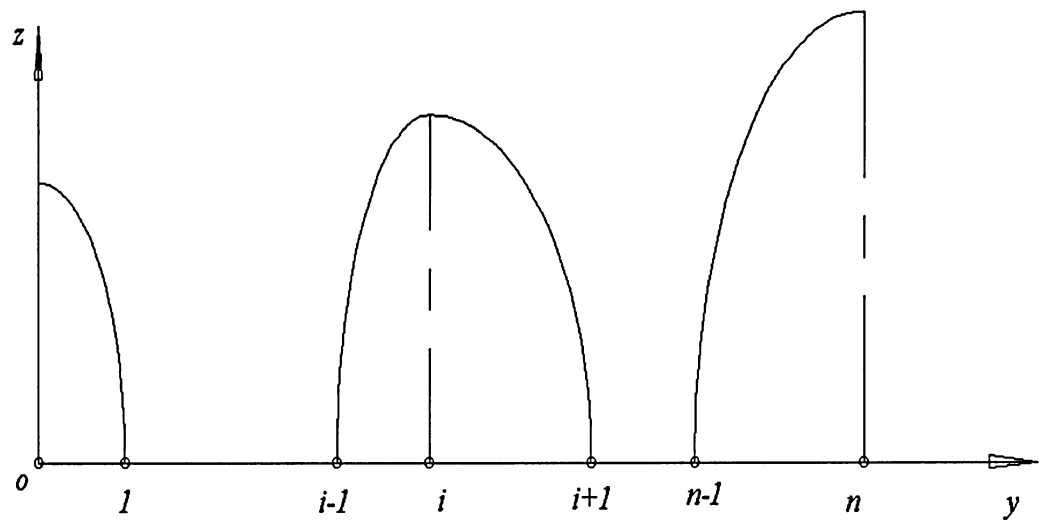

Figure 4-7. Illustration of nodes for three types of cutting grains

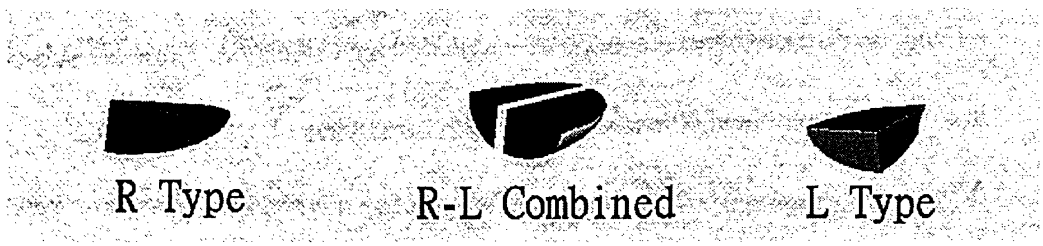

Figure 4-8: R-type, L-type, R-L combined type of ellipsoid chips

4.4 Generation of Workpiece Topography

With the last ellipsoid swept out from the workpiece, the simulation of grinding process is complete. What remains is to retrieve the topography of ground surface from the workpiece. For the topography data collection, the ray tracer module is employed to emit a vertical beam paralleling to *z* axis into the ground surface of the workpiece perpendicularly as illustrated in Figure 4-9. The distance from the source

to the hit point on the workpiece is returned, recorded and exported to a DAT file. To get a complete picture of the generated surface, the ground surface of workpiece is fully scanned by ray tracer module moving along x and y directions with constant feed rate. The collected data is exported to MATLAB, for plotting and calculating average roughness of the surface.

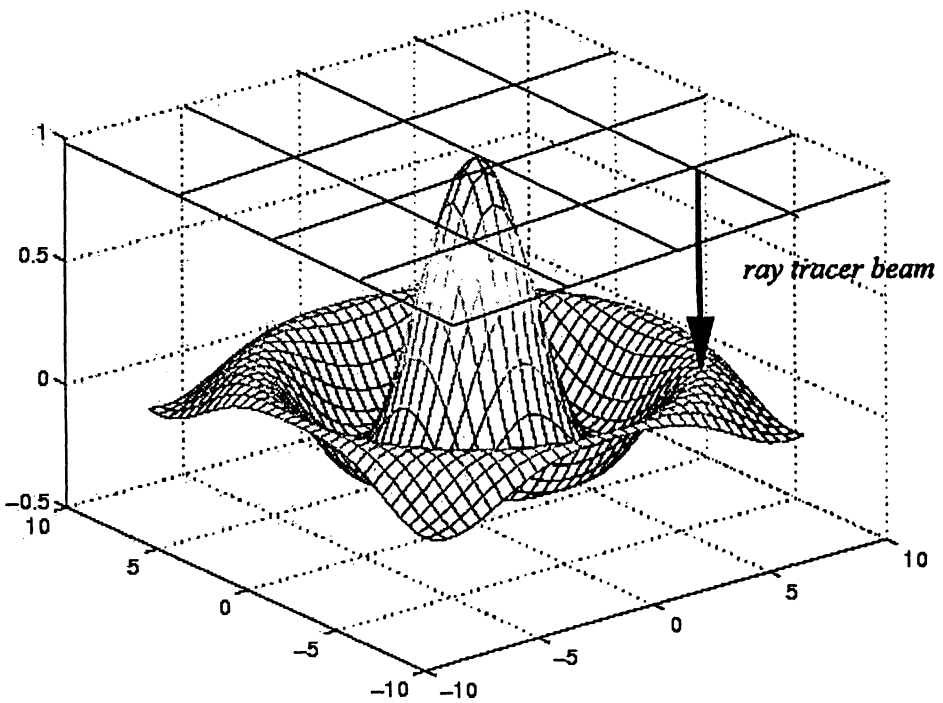

Figure 4-9. Illustration of Ray Tracer

4.5 Calculation of Surface Roughness

To assess the surface quality of the ground workpiece, surface roughness is measured. The most common methods of describing surface roughness in North America are the arithmetical average roughness R_a and root mean square (RMS)

roughness R_q. In this work, the arithmetical average roughness R_a is employed to characterize the quality of the finished surface. The average roughness calculation is conducted in the crossing direction of the lay, which is perpendicular to the moving direction of workpiece and grinding wheel (see figure 4-10). The average roughness is defined as:

$$R_a = \frac{1}{L}\int_{y=0}^{y=L} | z - z_0 | \, dy \tag{4-15}$$

in case of discrete data the following equation can be used:

$$R_a = \frac{1}{N}\sum_{1}^{N} | z_i - z_o | \tag{4-16}$$

where z is the ordinate of the profile from the centerline, and z_0 is the neutral line of the profile as illustrated in Figure 4-11.

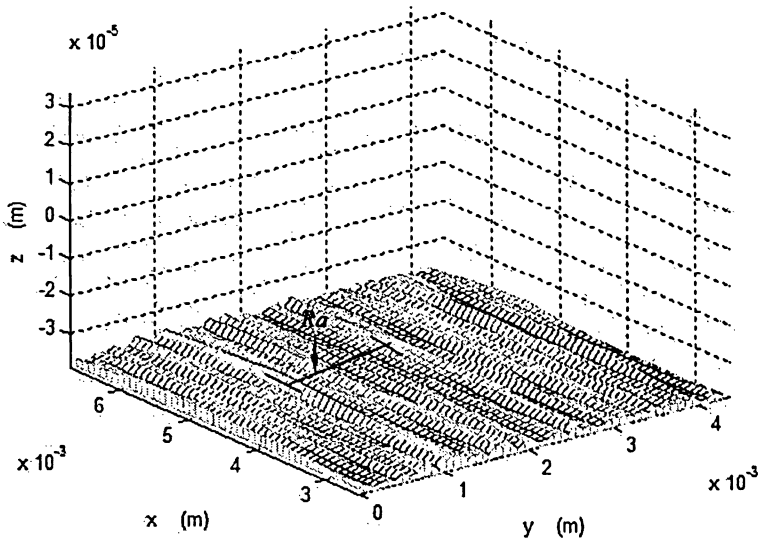

Figure 4-10. Illustration of calculation of average roughness

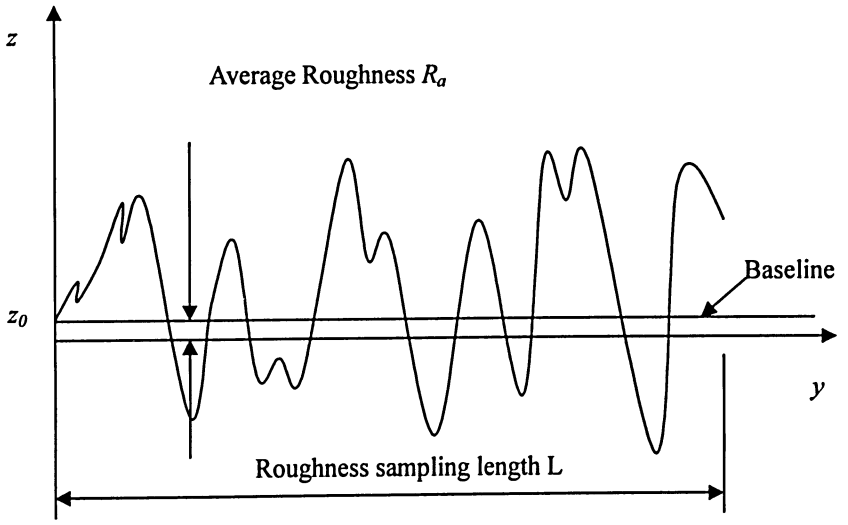

Figure 4-11. Designation of surface average roughness R_a

CHAPTER 5

RESULT AND DISCUSSION

5.1 Results

The proposed predictive model was experimentally evaluated by conducting grinding experiments using a Brand-G surface grinding machine. Three 1010 steel specimens are cut into 91.44 *mm* (length) by 25.4 *mm* (width). Each surface is ground under identical grinding conditions. The grinding wheel is dressed before the next surface is ground. The specifications of the grinding wheel were: 89A60J8AV217, i.e., the grit size of the grinding wheel was G60. The velocity of the workpiece was 25.4*mm/s* and the rotational speed of the grinding wheel was 2660*rpm*. The average roughness of ground specimens was measured by a stylus roughness gauge.

The predictive model was used four times with identical parameters to test the stability of the model predictions. Figure 5-1 shows the surface finish as predicted by the model. The mean average roughness of four runs varies between 3.2 μm to 4.3 μm; the maximum average roughness fluctuates between 4.9μm to 6.0μm. The minimum is from 2.1μm to 3.8μm.

Table 5-1 shows the experimental results for the average roughness of the ground

specimens. The average roughness measurements are between 2.92 μm to 3.36 μm with a mean value of 3.18μm. The average of the mean roughness for simulated results is 3.68 μm. The relative error for simulated results to the experimented results can be calculated as:

$$\varepsilon_t = \left|\frac{R_{a-s} - R_{a-e}}{R_{a-e}}\right| \times 100\% = \left|\frac{3.68 - 3.18}{3.18}\right| \times 100\% = 16.2\% \qquad (5\text{-}1)$$

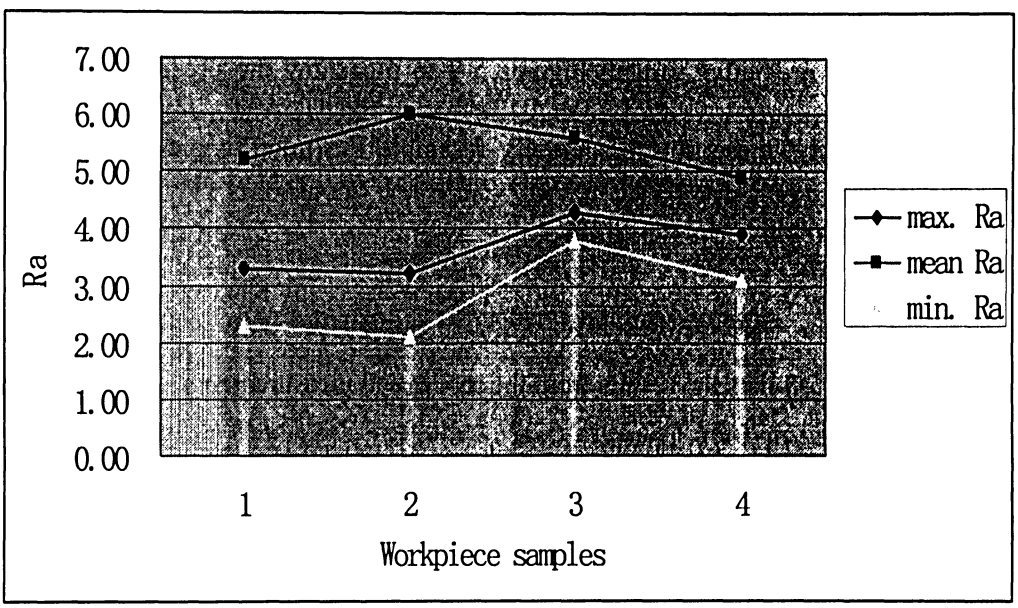

Figure 5-1. Four simulated results of average roughness

Table 5-1 Average roughness of workpieces ground by grinding machine

Workpiec No.	Ra(μm)	Ra(μm)	Ra(μm)	Ra(μm)	mean Ra(μm)
1	3. 24	3. 16	3. 28	3. 36	3. 26
2	3. 32	3. 12	3. 16	2. 92	3. 13
3	3. 12	3. 24	3. 00	3. 24	3. 15

Comparing the results of the model and experimental average roughness

measurements, it can be stated that the proposed model shows a high degree of accuracy.

5.2 Comparison with Literature

The proposed model was also compared with results published in the literature. Table 5-2 lists the grinding and wheel parameter used in the evaluation of the developed predictive model. Figures 5-2 to 5-5 show the predicted surface finish. Qualitatively, these surfaces closely resemble the microscopic topography of the finished ground surfaces [8][22].

Table 5-3 lists the results from the model and measurements reported in literature.

As seen from Table 5-3, the simulated average roughness R_a is fluctuating in range of 2.82 μm to 5.43 μm, with the mean value of 3.68 μm. Though they are bigger than the results from Zhou's [8] and Hwang's [22] work, which considered the wear of cutting grits, they are in the same order of magnitude. Thus, the simulation data in Table 5-3 is consistent with the previous work.

Table 5-2 Wheel and grinding parameters in simulation

Nominal wheel radius r_s:	150mm
Mean of grain size:	251 μm
Wheel spindle speed v_s:	2660rpm
Table speed v_w:	0.0254m/s
Number of grinding passes:	1
Cooling and lubrication:	dry
Dressing and grit wear:	not considered

Table 5-3 Comparison of simulated average roughness

	Simulated Data			Data in literatures	
	Minimum	Mean	Maximum	Zhou[8]	Hwang[22]
$R_a(\mu m)$	2.83	3.68	5.43	2.65[1]	1.5[2]

Note: 1: with wheel truncation of 2 μm, mean roughness of simulation results.

2: fresh grit without wear, mean roughness from experimental measurement

5.3 Results of the Simulated Finished Surfaces Topography

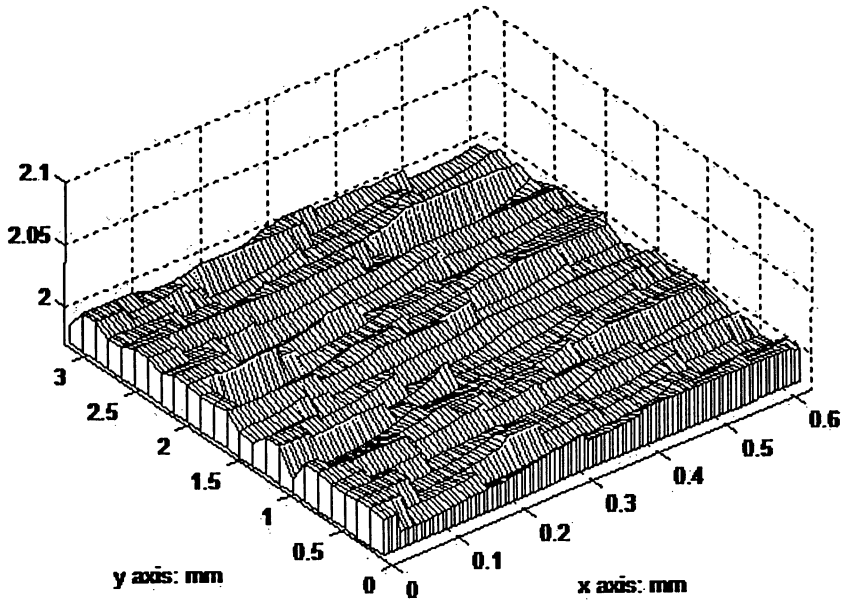

Figure 5-2. Simulated finished surface topography 1

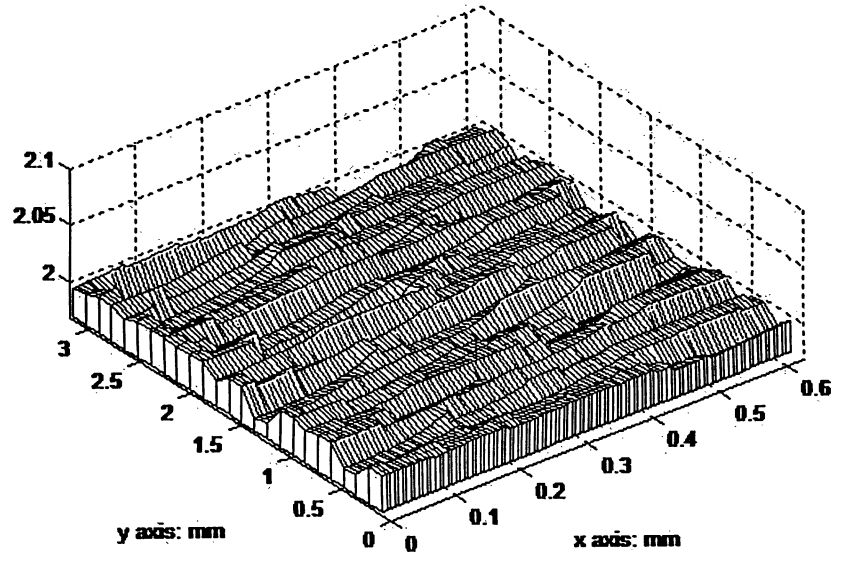

Figure 5-3. Simulated finished surface topography 2.

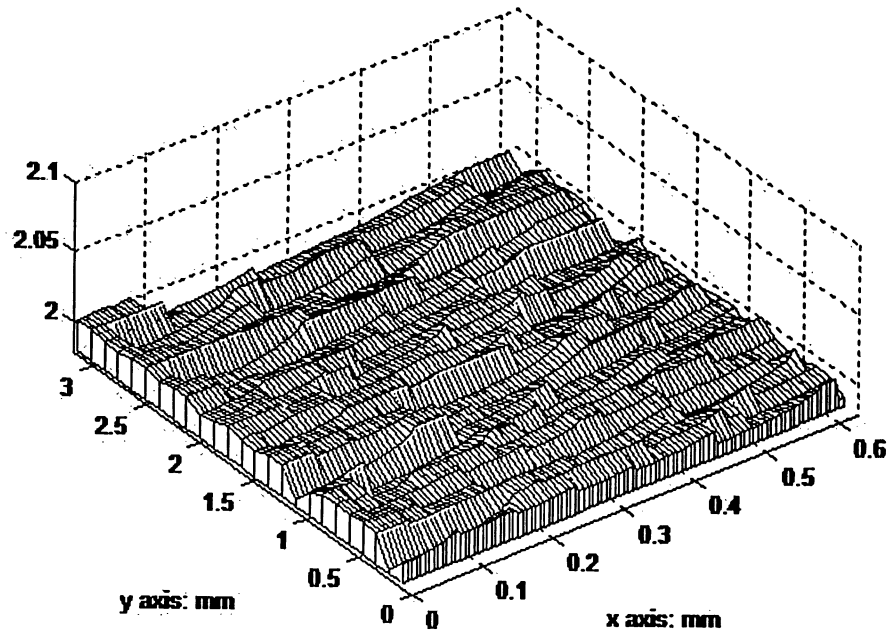

Figure 5-4. Simulated finished surface topography 3

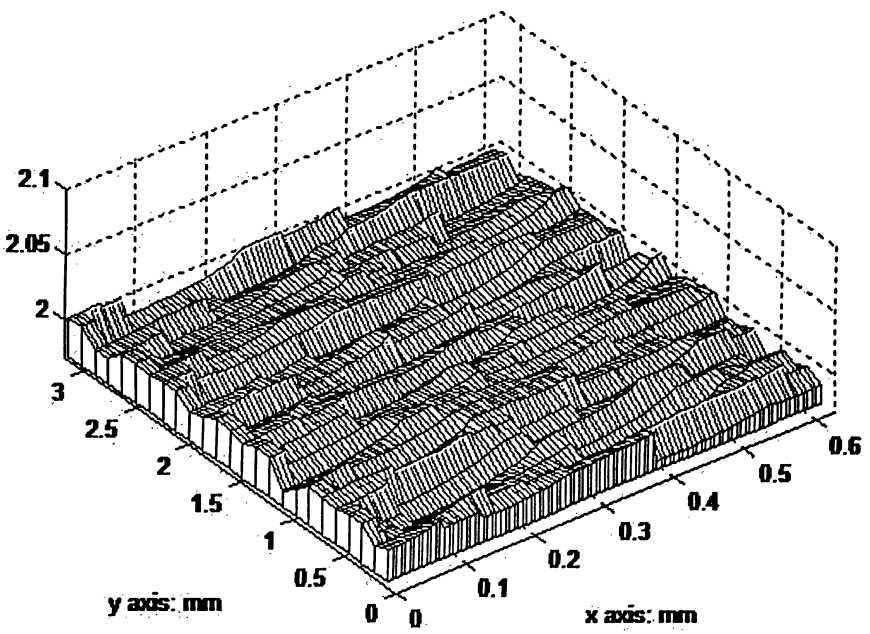

Figure 5-5. Simulated finished surface topography 4.

CHAPTER 6

CONCLUSIONS AND FUTURE WORK

6.1 Contributions

A novel, three-dimensional predictive model of chip formation in the fine grinding process has been developed. The model can be used to predict the surface finish of ground surfaces with acceptable accuracy.

6.2 Conclusions

A solid modeler was used for predictive modeling of surface finish in the grinding process. The model takes into account the statistical nature of the grinding process and the kinematics of the chip generation.

The proposed model was evaluated by comparing the predictions with measured surface roughness obtained through grinding experiments. The results showed the predictions were consistent with the measurements, hence proving the effectiveness of the model.

6.3 Future Works

The main improvement in the presented model would be to include gradual grain wear and the effects of the dressing and truing process. This would be especially useful in modeling a multi-pass grinding process.

REFERENCE

[1] S. Malkin, Grinding Technology: Theory and Applications of Machining with Abrasives, in: Ellis, Horwood (1989)

[2] M. C. Shaw, Principle of abrasive processing, Oxford University Press, (1996)

[3] H.K. Tönshoff, J. Peters, Inasaki, T. Paul, Modeling and Simulation of Grinding Process, Annals of the CIRP Vol. 41/2 (1992)

[4] X. Zhou, Modeling and Predicting Surface Roughness of the Grinding Process, Thesis for Master of Engineering Science, University of Western Ontario (2001)

[5] E. P. Degarimo, Material and Processes in Manufacturing (Ninth Edition), Wiley, (2000)

[6] J. Verkerk, Final Report concerning CIRP Cooperative Work in the Characterization of Grinding Wheel Topography, Annals of the CIPR 26 2, pp. 385 – 395 (1977)

[7] Tooe S., Umino K., Shinozaki N., Study on Grinding Characteristic of Grinding Wheel, Japan Society of Precision Engineering, Vol. 21, No. 4 (Dec. 1987)

[8] X. Zhou, F. Xi, Modeling and Predicting Surface Roughness of the Grinding Process, International Journal of Machine Tools & Manufacture 42, pp 967 – 977 (2002)

[9] Y. Namba, H. Tsuwa, Monte Carlo Simulation of Belt Grinding Process, Annals of the CIRP Vol. 25/1 (1976)

[10] W. Cooper, A. Lavine, Grinding Process Size Effect and Kinematics Numerical Analysis, ASME Journal of Manufacturing Science and Engineering, Vol. 122, pp.59-69 (2000)

[11] S. Tooe, K. Umimo, N. Shinozaki, Study on Grinding Characteristic of Grinding Wheel (1st Report), Bulletin of Japan Society of Precision Engineering, Vol. 21, No. 4, pp. 245-250 (1987)

[12] M. C. Shaw, A new theory of grinding, Int. Conf. Proc. Science in Inida, Monash University, Australia, pp. 1 – 16 (1971)

[13] X. Chen, W. B. Rowe, Analysis and Simulation of The Grinding Process, Part 2: Mechanics of Grinding, International Journal of Machine Tools & Manufacture Vol. 36, No. 8, pp. 883 – 996 (1996)

[14] G. Warnecke., U. Zitt, Kinematic Simulation for Analyzing and Predicting High-performance Grinding Processes, Annals of CIRP Vol. 47/1, pp. 265-270 (1998)

[15] I. Inasaki, Grinding Process Simulation Based on the Wheel Topography Measurement, Annals of CIRP, Vol. 45, pp 347-350 (1996)

[16] H. Yoshikawa, T. Sata, Simulated Grinding Process by Monte Carlo Method, Annals of the CIRP, Vol. 16 pp. 297-302 (1968)

[17] J. A. Badger, A. A. Torrance, A Comparison of Two Models to Predict Grinding Forces from Surface Topography, International Journal of Machine Tools & Manufacturer 40 pp. 1099 -1120 (2000)

[18] A. D. Spence, F. Abrari, M. A. Elbestawai, Integrated Solid Modeller Based Solutions for Machining, Computer Aided Design, Vol. 32 No. 8-9, pp. 553-568 (2000)

[19] A. D. Spence, Y. Altintas, A Solid Modeler Based Milling Process Simulation and Planning System, Trans. ASME, Journal Engineering for Industry, Vol. 116, pp. 61-69, (1994)

[20] W. P. Wang, K. K, Wang, Geometric Modeling for Swept Volume of Moving Solids, IEEE Computer Graphics and Applications, Vol 6 (12), pp. 8-17 (1986)

[21] K. V. Kumar, M. C. Shaw, A New Method of Characterizing Grinding Wheels, Annals of CIRP 28/1/1979, pp. 205-208 (1979)

[22] T. W. Hwang, C. J. Evans, S. Malkin, High Speed Grinding of Silicon Nitride with Electroplated Diamond Wheels, Part 2: Wheel Topography and Grinding Mechanics, Journal of Manufacturing Science and Engineering, February 2000, vol.122, pp. 42-50 (2000)

[23] http://www.robertnz.net/nr02doc.htm

[24] A. Bowyer, SVLIS Set---theoretic kernel modeler, Information Geometers, (1994)

APPENDIX A

Specification of Cobra DSR-2000 two-dimensional laser scanner

Model:	Cobra DSR-2000
Type:	Diffuse
Capture range:	2000 μm
Z accuracy within capture range:	10 μm
Dynamic resolution:	1.0 μm
Spot size:	32 – 48 μm
Standoff:	31.5mm